UNIVERSITÀ DEGLI STUDI DI PADOVA

UNIVERSITÀ DEGLI STUDI DI PADOVA

Dipartamento di
BIOMEDICINA COMPARATA E ALIMENTAZIONE

Corso di dottorato di ricerca in
SCIENZE VETERINARIE
Ciclo XXX

INTERACTION BETWEEN MAGNETIC NANOPARTICLES AND POLYPHENOLS AND APPLICATIONS IN THE FOOD INDUSTRY

Tesi redatta con il contributo finanziario della CAPES-Coordenação de Aperfeiçoamento de Pessoal di Nível Superior

Coordinatore:
Ch.mo Prof. (Alessandro ZOTTI)
Supervisore:
Ch.mo Prof (Fábio VIANELLO)

Dottoranda: JESSICA DE ALMEIDA ROGER

2017

ABSTRACT **4**

1-NANOTECNOLOGY **7**

2-NANOPARTICLES **7**

2.1-IRON OXIDE MAGNETIC NANOPARTICLES 8
2.1.1- Application of magnetic nanoparticles for biomolecule purification by magnetic separation 9
2.1.2- Application of magnetic nanoparticles for nanosensors 9
2.1.3- Application of magnetic nanoparticles as processing aid 10

3-NANOTECHNOLOGY IN FOOD INDUSTRY **11**

4-POLYPHENOLS **12**

4.1-CURCUMIN (CUR) 12
4.2-TANNIC ACID 13
4.3-NANOPARTICLES AND POLYPHENOLS 14

5-SAMNS **15**

5.1- SAMNS FOR CURCUMIN PURIFICATION 16
5.2- THE SAMN-TANNIC ACID COMPLEX FOR SENSOR DEVELOPMENT 17
5.3- PROCESSING AID BY THE SAMN-TANNIC ACID COMPLEX 18

6-AIMS **20**

7-RESULTS **21**

8-CONCLUSIONS **48**

9-REFERENCES **49**

ABSTRACT

The noticeable discoveries in the field of nanotechnologies of the last years emphasized the versatility of nanoscience in many fields. New evidences demonstrated that physical and chemical properties of nanomaterials can be tuned to reduce safety issues of nanotechnology applied in food industry. In this context, and inspired by the increasing interest of industry toward nanotechnology, a novel iron oxide magnetic nanoparticle, whose synthesis was developed in our laboratory, was used in association with polyphenols to elaborate hybrid nanomaterials with interesting applications in the food industry field. The magnetic nanoparticles, presenting a size around 10 nm and constituted of stoichiometric maghemite (γ-Fe_2O_3), were called Surface Active Maghemite Nanoparticles (SAMNs). SAMNs show a peculiar surface chemical behavior, which is highlighted by their high water stability as colloidal suspensions, without any superficial modification or coating derivatization. In addition, SAMN production is cost-effective and eco-friendly, and these nanoparticles can be advantageously reutilized. SAMNs are able to immobilize various biomolecules and the availability of iron (III) atoms on the particle surface provides to the nanomaterial the ability to selectively bind selected molecules. Thereby, upon molecule immobilization, a core-shell complex is formed, combining the magnetism of SAMNs (the core) and the function provided by the chosen molecule (the shell). Among several other biomolecules, phenolic compounds have a high affinity for maghemite nanoparticles. This occurs because the phenolic compounds have chelating groups that react with the iron (III) sites available on the surface of SAMNs. The immobilization of phenolic compounds on the surface of SAMNs is very stable and conserved upon binding, making it possible to use the resulting complex for various purposes, such as magnetic purification, drug delivery, etc. Thus, this study proposes the development of two hybrid nanostructure by coating SAMNs with tannic acid (TA) and curcumin (CUR). Both core-shell nanostructures, SAMN@TA and SAMN@CUR, presented high stability and were deeply characterized with different techniques. SAMN@TA was successfully applied for the creation of an electrochemical sensor for the detection of polyphenol content in blueberries by

square wave voltammetry. Furthermore, the antimicrobial properties of SAMN@TA were successfully tested on *Listeria monocytogenes*. Due to the effectiveness on reducing bacterial growth and easy removal from the system, SAMN@TA represents a possible alternative to antibiotic methods for the elimination of foodborne pathogens. Finally, the use of SAMN@CUR was proposed as a purification method to improve the extraction of pure curcumin from biological samples. The results demonstrated a sustainable and highly efficient magnetic purification process for curcumin as well as an outstanding yield of 90% and a purity > 98%. In conclusion, the reported multiple uses of SAMNs, ranging from biomolecule purification to foodborne pathogen control, offer valuable insights into the versatility of the nanomaterial and its potential applications in the food industry.

INTRODUCTION

1-NANOTECNOLOGY

The current nanotechnology revolution stimulated, through innovative prospects and applications, widely renovation possibilities for many science fields. Particular interest is focused on nanomaterial engineering, which provides a wide range of synthesis methods, due to the fact that this branch combines several structures and composition to create new materials. Among nanomaterials, nanoparticles are particularly interesting for their unique physical and chemical properties at nano-scale, that are the heart of the versatility of nano-sized materials (Wu, Mendoza-Garcia, Li, & Sun, 2016) that proved to be useful in fields as electronics (Bruce, Scrosati, Tarascon, Chemie, & Bruce, 2008) and biomedicine (Tian et al., 2017).

2-NANOPARTICLES

Nanoparticles are a wide class of materials that have a size in the 1-100 nm range and can be synthesized using different techniques. At nanoscale, materials present a variety of new properties, which further change with the size or the shape of the nanomaterial (Jasieniak, Califano, & Watkins, 2011). Actually, the unique nanoparticle features are scale-dependent, as an example, at size below 20 nm many features of the nanomaterial, including optical characteristic, magnetism, and the surface structure, can be altered (Burda, Chen, Narayanan, & El-Sayed, 2005; Iqbal, Iqbal, Li, Gong, & Qin, 2017). At this scale, the atom percentage on the surface increases exponentially in comparison to the same material in bulk phase, leading to a high exposition of functional atoms, and thus great reactive features (Whitesides, 2003; Wu et al., 2016).

Nanoparticles exhibit peculiar magnetic, electronic, and optical behavior, and offer the great advantage of a large reactive surface (Pérez-López & Merkoçi, 2011). Indeed enthusiastic efforts to understand and completely unveil these singular properties represent a crucial task nowadays

(Gupta & Gupta, 2005; Laurent et al., 2008; Lu, Salabas, & Schüth, 2007).

2.1-Iron oxide magnetic nanoparticles

Magnetic nanoparticles are commonly composed of iron oxide, and are a class of nanomaterials mostly represented by maghemite (γ-Fe_2O_3) or magnetite (Fe_3O_4). They can be synthetized advantageously at the size of the biological entities of interest (Pankhurst, Connolly, Jones, & Dobson, 2003). Besides the properties as low toxicity, biodegradability, small size, high surface area, and magnetism (Laurent et al., 2008; Lu et al., 2007), they present broad application possibilities due the wide spectrum of functionalities. Thereby, they can be used for biomedical applications in magnetic resonance imaging (MRI), for the efficient separation of biomolecules and as carriers for targeted drug delivery (Hola, Markova, Zoppellaro, Tucek, & Zboril, 2015; Magro et al., 2014; Wu, Mendoza-Garcia, Li, & Sun, 2016).

In particular, magnetic properties of iron oxides can be drastically influenced at the nano-size, resulting in the phenomenon of superparamagnetism, which consists in being responsive to an external magnetic fields without bearing residual magnetism at the end of the exposition (Gupta & Gupta, 2005). The magnetic manipulation, representing an effectively repeatable process, permits to readily remove the superparamagnetic material from the reaction vessel, allowing its subsequent dispersion in the system when magnetic field is absent (Govan & Gun ’ko, 2014). This property can be exploited to perform the magnetic separation and easy isolation of target substances in solution by simple application of an external magnetic field (Laurent et al., 2008).

Nevertheless, iron oxide nanoparticles present some important drawbacks, as this type of material normally exhibits a tendency to aggregate, presenting a low colloidal stability in aqueous media, hence the modification or coating derivatization to protect the nanoparticles surface is a necessary prerequisite (Govan & Gun ’ko, 2014; Gupta & Gupta, 2005; Kalkan, Aksoy, Aksoy, & Hasirci, 2012). Notwithstanding surface covering ensures stabilization of the nanomaterial, this additional

synthetic step limits possible nanoparticle applications at large scale, as it is a time consuming process, increasing of cost of the synthesis, as well as, due to the use of large volumes of solvents, it represents a source of environmental hazard (Mahmoudi, Sant, Wang, Laurent, & Sen, 2011).

2.1.1- Application of magnetic nanoparticles for biomolecule purification by magnetic separation

Magnetic separation techniques using nanoparticles represent an effective protocol for the separation and purification of specific molecules. In comparison with standard separation procedures, such as expensive liquid chromatography systems, this alternative technique is characterized by the facility, selectivity and reliability of the method, even for very large volumes (Horák, Babič, Macková, & Beneš, 2007; Safarik & Safarikova, 2004).

Even more interesting, the separation process can be performed directly on crude samples containing suspended solid material, thus, the purification process can be suitable to work in complex biological matrixes, like plants extracts. This advantage, with respect to standard chromatography techniques, reduces the quantities of solvents and avoid the dilution of the target molecule in solution. This technique is already used in chemical processing, waste remediation and purification system (Iranmanesh & Hulliger, 2017).

2.1.2- Application of magnetic nanoparticles for nanosensors

The wide range of applications of nanomaterials motivated great innovations also in the analytical technologies. For instance, the possibility to synthetize hybrid nanomaterials by combining nanoparticles with different functional components have attracted increasing interest, since the modification of physicochemical properties can enhance sensor stability, selectivity and sensitivity (Bülbül, Hayat, & Andreescu, 2015). Nanomaterials are intensely used in electronics, biomaterials sensing and, more recently, food industry (Pathakoti, Manubolu, & Hwang, 2017).

The large surface area and biocompatibility of iron oxide nanoparticles can be used as platform for immobilizing various types of molecules by means of physical adsorption or covalent binding

(Urbanova et al., 2014). This strategies permits to create novel bio-elements for developing new sensors responding to the request of the main goals of the specific research, offering good reproducibility and sensitivity (Bülbül et al., 2015). Electrochemical sensors based on iron oxide nanoparticles can be non-enzymatic, in which non-functionalized nanoparticles act as the sensing element. In addition, the magnetic recoverability, another advantageous nanosensor feature, permits the reuse of the system, representing in this way, an ecofriendly option to the expensive traditional methods. A significant range of application for sensors based on hybrid nanoparticles has been proposed, especially because of enhanced detection capabilities of analytical devices based on this technology (Viswanathan, Radecka, & Radecki, 2009).

2.1.3- Application of magnetic nanoparticles as processing aid

A processing aid is defined as a substance, not consumed as a food by itself, which is used in the processing of foods or their components, to implement a certain technological purpose during treatment or processing (Knorr et al., 2011). Recently, nanostructures have been suggested as a new processing aid in food productions process, in order to enhance food safety by reducing potential contamination during processing, as bacteriostatic/bactericidal agents or to facilitate an easier removal of impurities (Ansari, Grigoriev, Libor, Tothill, & Ramsden, 2009).

A successful application of nanoparticle as processing aid is represented by their application in the control of foodborne illness. For example, magnetic iron oxide nanoparticles were effectively tested on different types of microorganisms and the results indicated a high efficiency to separate the target bacteria from contaminated food (Huang, Wang, & Yan, 2010). The process can be developed using uncoated or functionalized nanoparticles, by attaching specific compounds (i.e. antimicrobials), on their surface (Varshney, Yang, Su, & Li, 2005; Yang, Qu, Wimbrow, Jiang, & Sun, 2007).

Once attached on bacterial cells, nanoparticles can induce membrane permeability, as their small size and highly reactive surface can cause stress and loss of bacterial membrane integrity, so that

the antimicrobial compound can be released from the nanoparticles inside the target microorganism (Ivanova, Fernandes, & Tzanov, 2013; Kafayati, Raheb, Angazi , Mahmoud Torabi Alizadeh, & Bardania, 2013). In addition, nanoparticles can penetrate the bacterial biofilm and hence disrupt this biological structure (Gholami et al., 2016; Taylor & Webster, 2011). Therefore, this novel non-traditional antimicrobial nanoparticle tool can help food industry to significantly reduce the possibility of disease outbreaks avoiding the emergence of drug resistance in bacteria caused due to excessive and inappropriate use of chemical substances (Arakha et al., 2015).

3-NANOTECHNOLOGY IN FOOD INDUSTRY

To face the worldwide increasing demand of food, technological advances for food processing and preservation are of fundamental importance. Food industry is constantly seeking for the development of new products and procedures to increase food offer in terms of nutritional and health values, safety and, and at the same time, to limit large scale waste production. In this context, nanotechnology applied to food industry represents a great innovation potential, attractiveness and profitability (Etheridge et al., 2013; Knorr et al., 2011).

The gradual progress of nanotechnologies and the increase of scientific knowledge regarding the control over their stability, physicochemical behavior and their safe manipulation demonstrate their suitability for food applications. Indeed, food industry is one of the sectors that most opened up the potential benefits of multi-faceted tools offered by nanotechnology (Livney, 2015).

Nano-formulates have been already used in food processing, such as food packaging, smart labels, nanosized ingredients and additives (Valdés, González, Calzón, & Díaz-García, 2009). Moreover, nanotechnology offers also innovative indirect pathways for upgrading the food productions, for instance, providing novel analytical tools, such as nanosensor, processing aids and selective purification procedures (Valdés et al., 2009).

4-POLYPHENOLS

Polyphenols are natural plant secondary metabolites showing multipotent combinations of biochemical activities. These powerful active compounds, constituting the plant defending system against pathogens and microorganisms, include simple or complex molecular structures that have in common the presence of aromatic rings and at least one hydroxyl function (Chung, Wong, Wei, Huang, & Lin, 1998).

The strong free radical scavenging action is probably the most important property of polyphenols. This grants to polyphenols a notable antioxidant activity, which is achieved by the direct scavenging of reactive oxygen species (ROS) and free radicals (Bhullar & Rupasinghe, 2013; Pan & Ho, 2008). Furthermore, these phytochemicals are recognized for their anti-inflammatory competence, antimicrobial, cardio-protective properties, promoting health and reducing the risk of several human chronic diseases (Ghosh, Banerjee, & Sil, 2015; Pan & Ho, 2008). In addition, polyphenols are abundant in natural sources, raising a great interest in medicinal and pharmaceutics industry.

4.1-Curcumin (CUR)

Among several polyphenols intensely studied, curcumin (Figure 1) is a natural compound extracted from rhizomes of *Curcuma longa* that possesses an incredible commercial potential because of its medicinal benefits, including imunopromotion, anticancer and chemoprevention properties (Gupta & Gupta, 2005). The medicinal use of curcuma has been extensively reported in Ayurveda (the Indian system of medicine) for over 6000 years (Aggarwal, Kumar &Bharti, 2003). Its wide use goes from the simple food spice and coloring agent to medicinal indication for multiple sclerosis and Alzheimer (Wanninger, Lorenz, Subhan, & Edelmann, 2015). Therefore, strategies for the improvement of the pure curcumin production, from plant cultivation to molecule isolation,

represent an important task and attract interest from food and pharmaceutical field (Green et al., 2008).

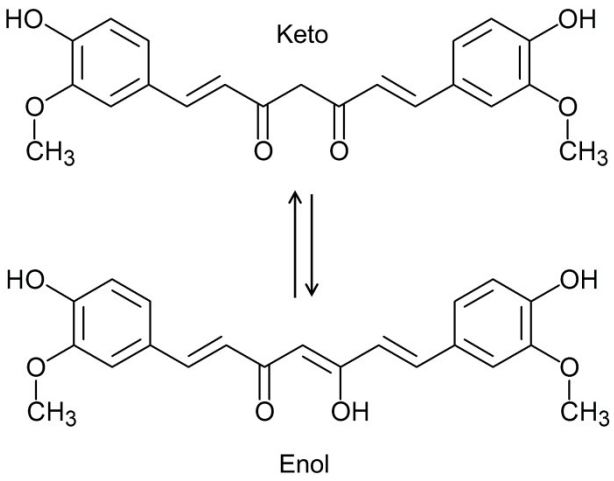

Figure 1. The molecular structure (schetch) of curcumin and its cheto-enol equilibrium.

4.2-Tannic acid

Tannins are usually classified into two groups: proanthocyanidins and hydrolysable tannins. Proanthocyanidins are flavonoid oligomers of catechin and epi-catechin and their gallic acid esters. Hydrolysable tannins are composed of gallic and ellagic acid esters of core molecules that consist of polyols, such as sugars, and phenolics, such as catechin. Tannic acid (P-penta-O-galloyl-d-glucose) (Figure 1) is the model compound for this group of tannins (Chung, Wong, Wei, Huang, & Lin, 1998). Tannins compounds were used in many industrial applications and as component of cosmetic products and pharmacological drugs due to their antioxidant activity, antimutagenic, and anticancarcinogenic properties (Roche et al., 2015).

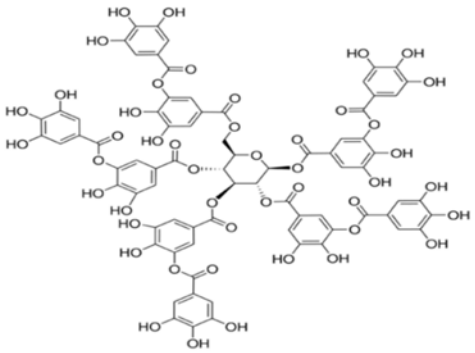

Figure 2. Molecular structure of tannic acid

4.3-Nanoparticles and polyphenols

Nanotechnology can provide useful and effective devices for determining phenolic compounds in various industrial processes. For example, phenols are commonly measured in environmental settings using expensive and time-consuming methods that include colorimetric, gas chromatography and liquid chromatography (Kitts & Weiler, 2003). In this context, new nanotechnology based techniques can offer cost-effective, fast and sensitive detection devices permitting easier evaluation of the safety limits of the phenolic present in waste water and environmental matrices (Faraji, 2016).

The use of nanotechnology-based systems has been proposed as a convenient solution to enhance the bioavailability of polyphenol molecules, while still maintaining their structural integrity (Etheridge et al., 2013). Nanoparticles has been mentioned as an alternative approach to enhance the polyphenol protection from degradation and to increase their shelf life (Musthaba, Baboota, Ahmed, Ahuja, & Ali, 2009). Finally, the ability of nanoparticles to behave as carriers for molecules, in combination with metal chelating properties of polyphenols, can be exploited for the development of separating/isolating systems providing novel green routes to produce advanced functional materials (Hu, Liu, Zhang, & Zeng, 2017; Mai & Hilt, 2017).

5-SAMNs

Being aware of the importance of sustainable procedures for the synthesis of nanomaterials, a novel wet synthesis pathway for producing a new type of superparamagnetic nanoparticles was recently developed by our research group (Magro, Valle, Russo, Nodari, & Vianello, 2012b). The innovative material consists of stoichiometric maghemite (γ-Fe_2O_3), with unique spectroscopic properties, size around 10 nm and well-defined crystalline structure (Magro, Faralli, et al., 2012; Magro, Sinigaglia, et al., 2012). This nanomaterial, denominated "Surface Active Maghemite Nanoparticles" (SAMNs), exhibits a peculiar ability to form stable colloidal suspensions in water without any organic or inorganic coating, being freely stable for several months as colloidal suspensions, and presents a high average magnetic moment (Bonaiuto et al., 2016).

In addition, SAMNs present the property of specifically bind organic molecules, leading to composite colloidal nanomaterials (Magro, Faralli, et al., 2012). The peculiar surface chemistry of SAMNs can be explained by the presence of under-coordinated Fe (III) atoms distributed on SAMN surface, which act as binding sites for molecules presenting chelating functionalities, such as hydroxyl or phosphate groups, keto-enol or isothiocynate moieties on their structure (Sinigaglia et al., 2012).

The functionalization process of SAMNs involves the self-assembly of a monolayer of a particular compound on the nanoparticles surface, which occurs by simply incubation in aqueous solutions (Magro, Faralli, et al., 2012). Thus, the selectivity of SAMN surface reduces the absorption of nonspecific compounds and confers a high specificity. Furthermore, the functionalization process does not interfere with the magnetic properties of SAMNs.

Bare SAMNs display an excellent recycling availability, long lifetime, selectivity and stability (Baratella et al., 2017; Chemello et al., 2016; Urbanova et al., 2014), and they can be considered as an excellent environmental friendly and cost-effective tool for various industrial applications. In particular, the recycling potential is an important industrial issue as the reusability of nanoparticles added to long lifetime are extremely required for this sector (Molnár & Papp, 2017).

Furthermore, SAMNs show notable electrocatalytic properties, already been used for the construction of electrochemical sensors (Urbanova et al., 2014) and biosensors (Baratella et al., 2013). Finally, successful interactions of SAMNs with organic and inorganic molecules led to the creation of nano-conjugates with novel properties that have already been exploited in several fields, ranging from drug delivery (Chemello et al., 2016) polyamine detection in tumor tissue (Bonaiuto et al., 2016), biomarker recognition (Miotto et al., 2016), contrast agent for MRI (Skopalik et al., 2014). For all the reasons, SAMNs represent the ideal candidate for exploring numerous novel applications.

5.1- SAMNs for curcumin purification

Effective magnetic purification of biomolecules is one of the most interesting application of SAMNs for the pharmaceutical and food industries. Due their unique properties, the reactive surface of SAMNs offers a high specificity to select iron-chelating molecules (Magro et al., 2014). SAMNs preserved crystalline structure upon binding and the ability to release molecules make them an attractive novel tool for isolating and purifying substances from natural matrixes (Magro et al., 2014).

Curcumin presents keto-enol functionality, hence it exhibits a good binding proclivity toward SAMN reactive surface. On these bases, Magro et al. (2014) demonstrated the application of SAMNs to purify curcumin from complex matrixes without any kind of preparation step. Presenting a fast and ecologically green production, involving the reduction of solvent volumes and offering the possibility to reuse SAMNs for several purification cycles, this technique provides an interesting example of the utilization of magnetic nanoparticles for biomolecule purification. However, other aspects need to be taken into consideration regarding the purification techniques of curcumin. For instance, an evaluation of the influence of environmental factors and agronomic techniques on plant cropping is crucial for improving the content of curcumin in the plant (Kitts & Weiler, 2003). In this context, to improve the curcumin production, it is very important to

understand in which phase of plant development can lead to the recovery of highest amount of curcumin in the biological matrix. A multidisciplinary approach, ranging from agronomy to nanotechnology, could offers valuable insights for a sustainable production of pure curcumin from a laboratory scale to industrial level.

5.2- The SAMN-tannic acid complex for sensor development

The desired goals for next generation sensors includes the optimization, at the same time, of sensitivity, specificity and real-time detection. SAMN-based sensors are simple, cost effective, potentially suitable for in-field readable responses and they can detect with high accuracy relevant target species (Baratella et al., 2017; Bonaiuto et al., 2016). Recently, researches empathized the application of polyphenolic compounds to modify the surface of nanoparticles to be used as sensors. Among polyphenols, tannic acid (TA) presents a particular structure with hydroxyl groups which offer the ability to form molecular interactions to form layers on nanoparticles surface (Abouelmagd, Meng, Kim, Hyun, & Yeo, 2016). TA interacts with iron oxide crystalline forms including lepidocrocite (γ-FeOOH), goethite (α-FeOOH), magnetite (Fe_3O_4) and, of course maghemite (γ-Fe_2O_3). TA easily binds Fe^{3+} ions leading to the formation of complexes of known low solubility in water. In fact, precipitating ferric tannates form a protective layer with inhibiting corrosion on metallic iron and steel.

The development of stable and functional interfaces of nanostructured ferric tannate on peculiar maghemite nanoparticles occurs by self-assembly in aqueous solution producing a novel nanoarchitecture called SAMN@TA. Due to its high structural stability and its electrochemical properties, SAMN@TA could be applied for the development of a modified electrode aimed at the electro-oxidation of polyphenols, which widened the application possibilities of both TA and maghemite nanoparticles due to a synergistic effect.

5.3- Processing aid by the SAMN-tannic acid complex

A different biotechnological application of SAMNs included its use as a processing aid in food industry, exploiting the physical-chemical properties of magnetic nanoparticles and their propensity to spontaneously bind on microorganism membrane (Azam et al., 2012). Moreover, the reactive surface of SAMNs can be coated with antimicrobial compounds, which, in turn, enhance antimicrobial effectiveness (Grumezescu et al., 2010; Huang, Wang, & Yan, 2010; Raghupathi, Koodali, & Manna, 2011).

Because of the size and high surface-volume-ratio of SAMNs, showing affinity for bacteria cell, these nanoparticles can bind to the bacterial surface (Martinez-Gutierrez et al., 2010). This powerful interaction can cause the clustering of bacteria cells that, combined with the magnetic property of SAMNs, can be used to remove the aggregates from the system using an external magnetic field (Ansari, Grigoriev, Libor, Tothill, & Ramsden, 2009; Gholami et al., 2016). This procedure could be considered as a new non-thermal process to remove bacteria from the environment (cleaning purpose) or to increase the stress effect of sanitizing agents on bacteria due to the stretching effect of the magnetic field application (Taylor & Webster, 2011; Xu, Li, Zhu, Huang, & Zhang, 2014). These new applications can reduce the use of classical sanitizers and disinfectants and can reduce the use of preservatives on food.

Among phenolic compounds, tannic acid stands outs for an effective inhibition of the growth of Gram-positive bacteria (Payne et al., 2013). As tannic acid (TA) and SAMNs form an extremely stable hybrid nanostructured complex, we tested SAMN@TA on *Listeria monocytogenes.*

L. monocytogenes is a Gram-positive foodborne bacterium that can cause relatively uncommon infections with, in most cases, mild symptoms. However, the fatality rate van reach 30% among at-risk patients (Ramaswamy et al., 2007). Notwithstanding sanitization efforts have significantly reduced the contamination by *L. monocytogenes*, the incidence of illness outbreaks in susceptible populations, as pregnant woman, remained constant along the years (Buchanan, Gorris, Hayman,

Jackson, & Whiting, 2017). Therefore, investigating the antimicrobial properties of SAMN@TA on *Listeria monocytogenes* in comparison to free TA, can give important information about the preservation of TA's inhibitory activity when bound on nanoparticles as the immobilization of compounds of interest on the nanoparticle surface can intensify the effects on the target pathogens (Taylor & Webster, 2011). For instance, phenolic compounds, that have the ability to interfere with the bacterial growth and are promising anti-biofilm agent (Miklasińska et al., 2016; Min, Walker, Tomita, & Anderson, 2008), would become great candidates to be used as natural antibacterial agents upon immobilization on nanoparticles (Ivanova, Fernandes, & Tzanov, 2013).

Moreover, magnetic nanoparticles offer the possibility of being magnetically removed, leaving no residues into the food matrix, making this nano-carrier an innovative processing aid for surface treatments. Therefore, the carrier properties of SAMNs could be used to improve the antimicrobial efficiency by increasing the compound bioavailability and, moreover, offering the advantage of being magnetically drivable. In addition, SAMN@TA could be used as an effective, low-cost and environmental friendly antimicrobial nanomaterial for applications in the food industry.

6-AIMS

The main objective of this thesis was to study and characterize the physical and chemical properties of iron oxide nanoparticles in combination with polyphenols in order to elaborate hybrid nanomaterials for the development of novel applications in the food industry field. More in-depth, the specific objectives were to:

1) Study the purification method for the recovery of curcumin present in the mother biological matrix (*Curcuma longa* root) using magnetic nanoparticles (SAMNs). In addition, the scaling up at industrial level of the proposed approach was demonstrated by developing an automatic modular pilot plant, which was able of performing the continuous curcumin purification from the initial water-ethanol extract of the *C. longa* root. The proposed multidisciplinary approach embodies the fundamental principles of clean production, providing a paradigm for the utilization of magnetic nanoparticles for biomolecule purification.

2) Examine the development of nanostructured ferric tannate, using tannic acid (TA) interfaces on peculiar maghemite nanoparticles (SAMNs) to produce the SAMN@TA complex. The structure and the electrochemical properties of the nanostructured material were characterized and applied for the development of a novel sensing electrode that was proved to electro-oxidation of polyphenols. The peculiar electrochemical properties of the SAMN@TA nanosensor were successfully used for the determination of polyphenols in real samples, representing a potential alternative to classical techniques.

3) Investigate the antimicrobial properties of the SAMN@TA hybrid nanostructure against the bacterium *Listeria monocytogenes.* In particular, the antimicrobial properties of SAMN@TA on *Listeria monocytogenes*, in comparison with free TA, can give important information about the preservation of TA's inhibitory activity when bound on nanoparticles. Thus, SAMN@TA was proposed as processing aid for surface treatment, without leaving residues, for food industry.

7-RESULTS

7.1- A purification system developed to offer valuable insights for a sustainable production of pure curcumin at an industrial scale and for the economic valorization of agro-industry.

Publication number 1:

Ferreira, M. I. Magro, M. Ming, L. C. Silva, M. B. Da. Rodrigues, L. F. O. S. Prado, D.Z. do. Bonaiuot, E. Baratella, D. **De Almeida Roger, J**. Lima, G.P.P. 2017. Rossetto, M. Zennaro, L. Vianello, F. Sustainable production of high purity curcumin from Curcuma longa by magnetic nanoparticles: A case study in Brazil. Journal of Cleaner Production. 154:233-241.

Journal of Cleaner Production 154 (2017) 233–241

Contents lists available at ScienceDirect

Journal of Cleaner Production

journal homepage: www.elsevier.com/locate/jclepro

Sustainable production of high purity curcuminoids from *Curcuma longa* by magnetic nanoparticles: A case study in Brazil

Maria Izabela Ferreira [a, 1], Massimiliano Magro [b, c, 1], Lin Chau Ming [d], Monica Bartira da Silva [d], Luan Fernando Ormond Sobreira Rodrigues [d], Débora Zanoni do Prado [a], Emanuela Bonaiuto [b], Davide Baratella [b], Jessica De Almeida Roger [b], Giuseppina Pace Pereira Lima [a], Monica Rossetto [e], Lucio Zennaro [e], Fabio Vianello [b, c, *]

[a] Department of Chemistry and Biochemistry, São Paulo State University (UNESP), Institute of Biosciences, Botucatu, São Paulo, CP 510, 18.618-970, Brazil
[b] Department of Comparative Biomedicine and Food Science, University of Padua, Padua, Italy
[c] Regional Centre of Advanced Technologies and Materials, Department of Physical Chemistry and Experimental Physics, Faculty of Science, Palacky University, 17 Listopadu 1192/12, 771 46 Olomouc, Czech Republic
[d] Department of Horticulture São Paulo State University (UNESP), School of Agriculture, Botucatu, São Paulo, CP 510, 18.618-970, Brazil
[e] Department of Molecular Medicine, University of Padua, Padua, Italy

ARTICLE INFO

Article history:
Received 24 January 2017
Received in revised form
23 March 2017
Accepted 29 March 2017
Available online 31 March 2017

Keywords:
Turmeric
Curcumin production
Curcumin purification
Magnetic purification
Magnetic nanoparticles
Biomass reduction

ABSTRACT

Large volumes of residual biomass could represent a matter of concern for large-scale purification of natural compounds, heavily influencing processing industries and logistic sizing, amount of solvents employed for the extraction processes and the final chemical and biological waste generation. In the present study, carried out in Brazil, the production of curcuminoids in *Curcuma longa* L. rhizomes was maximized as a function of plant maturity and solar UV exclusion. Noteworthy, curcuminoid content reached its maximum at around the end of the early vegetative phase (65 days after planting), henceforward plant growth determined only a detrimental accumulation of wastes. The harvesting at this early phase of plant maturation led to a more than tenfold reduction of exceeding biomass. In addition, by means of an innovative, sustainable and high efficient magnetic purification process for curcuminoids based on Surface Active Maghemite Nanoparticles (SAMNs), an outstanding yield of 90% and >98% purity, were achieved in a single magnetic purification step. The formation of the SAMN-curcuminoid complex (SAMN@curcuminoid) was demonstrated by optical and electron spin resonance spectroscopy and electron microscopy. The scalability of the purification method was proved by the application of an automatic modular pilot system for continuous magnetic purification of curcuminoids, capable of managing 100 L day^{-1} of SAMN@curcuminoid suspensions. The presented multidisciplinary approach embodies the fundamental principles of cleaner production providing a paradigm for the utilization of magnetic nanoparticles for biomolecule purification. Moreover, Brazilian agro-industries can benefit from sustainable innovation strategy outlined by the current study.

1. Introduction

The rational use of natural resources, the minimization of wastes as well as the sustainable product innovation are prerogatives of the research field on cleaner production. *Curcuma longa* (Zingiberaceae), also known as turmeric, is the most important source of curcuminoids, comprising curcumin and two related compounds, demethoxycurcumin (DMC) and bisdemethoxycurcumin (BDMC) (Kulkarni et al., 2012). Nowadays, curcumin is used as a food supplement in several countries and the molecular basis for its pharmaceutical application has been already delineated for a wide range of diseases (Gupta et al., 2013). For this reason, curcumin and

* Corresponding author. Department of Comparative Biomedicine and Food Science, University of Padua, Agripolis - Viale dell'Università 16, Legnaro, 35020, PD, Italy.
E-mail address: fabio.vianello@unipd.it (F. Vianello).
[1] Authors contributed equally to this work.

http://dx.doi.org/10.1016/j.jclepro.2017.03.218
0959-6526/

its derivatives are attracting an increasing interest in food and pharmaceutical field. Thus, the development of strategies for the improvement of pure curcuminoid production, from plant cultivation to molecule isolation, represents an important task. From this viewpoint, the influence of environmental factors and agronomic techniques on plant cropping is an important research topic, as these factors influence the accumulation of biomass as well as the biosynthesis of bioactive compounds.

In the present report, in the specific agro-climatic zone, under the effect of different light intensities and UV exclusion, the curcuminoid content in rhizomes reached its maximum at approximately the end of the early vegetative phase. Henceforward, the amount of curcuminoids did not significantly vary with plant growth. Thus, the anticipation of the harvest led to a significant waste minimization and a one order of magnitude lower biomass accumulation. Moreover, a sustainable and competitive purification procedure was developed in the present study. Pharmaceutical and food industries usually employ various chromatographic, ultrafiltration, or precipitation techniques or solvent extraction methods for isolating biomolecules of interest (Kitts and Weiler, 2003). These techniques show significant drawbacks when applied at the industrial scale, such as expensive instrumentation, time-consuming procedures, or large quantities of organic solvents and corresponding wastes. In particular, the main disadvantage of all standard column liquid chromatography procedures is the impossibility to cope with biological samples containing particulate material, so these techniques are not suitable for working at the early stages of the isolation/purification process, when suspended solids and fouling components are present in the sample (Turková, 1978). In this context, the use of magnetic nanoparticles can represent a valuable option as well as an innovation opportunity for cleaner production. Notwithstanding, most of the proposed syntheses of magnetic nanoparticle drastically limit their exploitation at an industrial level, as they are characterized by difficult scalability, impressive consumption of organic solvents, high costs and heavy impact on the environment. Furthermore, magnetic nanoparticles need in the most of the cases, to be stabilized to avoid self-aggregation and to guarantee long-term stability, pH and electrolyte tolerance, and proper surface chemistry. Coating processes are often cumbersome, time-consuming, and expensive, with low yields and, due to their lack of stability, coating tend to degrade. Coating deterioration represents a drawback as this phenomenon compromises the binding capability of the material. As a consequence, the use of nanomaterials as means for cleaner production could reasonably become a paradox, as they represent themselves sources of environmental hazard.

Recently, we developed a novel synthetic procedure for magnetic nanomaterial in the size range around 10 nm, constituted of stoichiometric maghemite (γ-Fe_2O_3) and showing peculiar surface chemical behavior, called surface active maghemite nanoparticles (SAMNs) (Magro et al., 2015a). Noteworthy, SAMNs applicability range from the biomedical field, as a long-term imaging nanoprobes (Cmiel et al., 2016; Skopalik et al., 2014), to the advanced material development, such as conductive DNA based metamaterials (Magro et al., 2015b) and electrocatalysis (Magro et al., 2016a), as well as in sensoristics (Urbanova et al., 2014) for the determination of glucose (Baratella et al., 2013), polyamines (Bonaiuto et al., 2016) and hydrogen peroxide (Magro et al., 2013, 2014a). SAMNs present a high average magnetic moment and high water stability as colloidal suspensions without any superficial modification or coating derivatization. Because of their unique physical and chemical properties, these naked iron oxide nanoparticles are currently used to immobilize various biomolecules, such as avidin (Magro et al., 2012a), curcumin (Magro et al., 2015c), citrinin (Magro et al., 2016b), rhodamine B isothiocyanate (Sinigaglia et al., 2012) and endogenous proteins from prokaryotes and eukaryotes (Magro et al., 2016c; Miotto et al., 2016; Venerando et al., 2013). Thus, SAMNs represent an ideal material for cleaner production as their synthesis is scalable and completely carried out in water. They do not need any kind of stabilizing coating, present a very high aqueous colloidal stability and, in contrast to their surface reactivity, they are structurally conserved upon binding to target molecules, such as curcumin (Magro et al., 2014b), DNA (Magro et al., 2015b) and chromate (Magro et al., 2016e).

In the present work, a purification method leading to the recovery of curcuminoids present in the mother biological matrix with high yield (90%) and purity (98%) was proposed. In addition, the feasibility of the proposed approach to be scaled up at industrial level was demonstrated by developing an automatic modular pilot plant, which was able of performing the continuous curcuminoid purification from the initial water-ethanol extract. The reported multidisciplinary approach, ranging from agronomy to nanotechnology and engineering, offers valuable insights for a sustainable production of pure curcuminoids at an industrial scale and for the economic valorization of Brazilian agro-industry.

2. Materials and methods

2.1. Materials

The cultivation experiments were carried out in an experimental farm of the Agronomic Science College, Universidade Estadual Paulista - UNESP, Botucatu - SP, in São Manuel - SP (22°46′0,571″ S and 48°34′11,32″ W, 744 m above sea level).

The experimental design was completely randomized with five light conditions and four harvest times, split plot in time, with five replicates consisting of six plants. Light levels were: A) UV exclusion; B) full sun, C) 30% shading; D) 50% shading and E) 70% shading. Harvest times were: 65, 128, 174, and 203 days after planting (DAP) corresponding to January, April, May, and June 2013.

The different light conditions were obtained by protected environments in tunnel structures, 3 m wide, 1.70 m high and 22.5 m long, with different coatings for light exposure control. The coating applied to exclude UV radiations was an anti-UV polyethylene film (150 μm) (Trifilme, Plastilux, Brazil), characterized by excluding more than 80% UV-B radiation. Coatings used to control shading levels were black polyethylene screens with 30%, 50% and 70% shading (Plastilux, Brazil).

An infrared gas analyser (LI-6400, Li-Cor Inc. Lincholn, NE, USA) was used to quantify photosynthetically active radiation (PAR). Measurements were carried out at 09:00 and 11:00 a.m. in cloudless days, every month during the plant growth. The mean PAR measured was used to define the amount of radiation for each light exposure condition: UV exclusion (610 μmol $m^{-2}s^{-1}$), 70% shading (360 μmol $m^{-2}s^{-1}$), 50% shading (500 μmol $m^{-2}s^{-1}$), 30% shading (630 μmol $m^{-2}s^{-1}$) and full sun (1200 μmol $m^{-2}s^{-1}$).

The soil was classified as Oxisol, sandy phase (Camargo et al., 1987; Santos et al., 2006) and exhibited the following chemical characteristics in the layer between 0 and 0.20 m: 12 g dm^{-3} organic matter; pH 5.4; 204 mg dm^{-3} P; 2.5 mmol dm^{-3} K; 39 mmol dm^{-3} Ca; 11 mmol dm^{-3} Mg; 71 mmol dm^{-3} CTC; V = 76%.

Seed rhizomes, 12 cm long, were selected and homogenized. Planting was carried out on plots 0.4 m high, spaced 0.5 m apart, by placing each propagule 4 cm deep.

Necessary crop treatments, such as weed control and repairs in ridges were carried out during plant growth. Plots were irrigated daily, according to water demand recorded by tensiometers, thus soil was near its calculated field capacity. Irrigation was suspended 15 days before harvest.

Rhizomes of six plants for each replica were harvested, sliced and dried in a forced air-circulating oven at 65 ± 5 °C until the samples reached a constant weight to determine biomass production, expressed per plant. These dried rhizomes were milled to a fine powder, pooled, mixed and used to measure the curcuminoid content by HPLC. The water content in the fresh rhizomes was approximately 83 ± 3%.

2.2. Chemicals

Chemicals were purchased at the highest commercially available purity, and were used without further treatment. Iron(III) chloride hexahydrate (97%), sodium borohydride ($NaBH_4$), and ethanol (99.6%) were obtained from Aldrich (Sigma-Aldrich, Italy) as well as pure curcuminoids (curcumin, demethoxycurcumin, and bis-demethoxycurcumin) (purity ≥ 94.0%), being curcumin ≥80.0% (by TLC). HPLC grade ethanol, acetonitrile and acetic acid were from Mallinckrodt (St. Louis, USA).

2.3. Instrumentation

Optical spectroscopy measurements were performed in 1 cm quartz cuvettes using a Cary 60 spectrophotometer (Varian Inc., Palo Alto, CA, USA).

Electron spin resonance spectra were acquired in water, in a glass tube (50 μL), at room temperature (21 °C), by a Bruker ER200D X-band ESR spectrometer (Bruker, Germany). Experimental parameters were: magnetic field modulation 100 kHz; power, −10 dB (20 mW); frequency, 9.84 GHz; scan rate, 20 Gauss s^{-1}; modulation amplitude, 1 Gauss; time constant, 1 s. The center field values were calibrated and locked by using the stable free radical 2,2-diphenyl-1-picrylhydrazyl (DPPH), 50 μM, as internal standard.

A series of Nd − Fe − B magnets (N35, 263–287 kJ/m^3 BH, 1170–1210 mT flux density by Powermagnet, Germany) was used for the magnetic driving of nanoparticles.

2.4. Synthesis of surface active magnetic nanoparticles

A typical synthesis of nanoparticles was already described and can be summarized as follows (Magro et al., 2012b, 2015a): $FeCl_3 \cdot 6H_2O$ (10.0 g, 37 mmol) was dissolved in Milli-Q grade water (800 mL) under vigorous stirring at room temperature. $NaBH_4$ solution (2 g, 53 mmol) in ammonia (3.5%, 100 mL, 4.86 mol mol^{-1} Fe) was quickly added to the mixture. Soon after the reduction reaction occurrence, the temperature of the system was increased to 100 °C and kept constant for 2 h. Then, the material was cooled at room temperature and aged in water, as prepared, for 24 h. This product was separated by imposition of an external magnet and washed several times with water. This material can be transformed into a red-brown powder (final synthesis product) by drying and curing at 400 °C for 2 h. The resulting nanopowder showed a magnetic response upon exposure to a magnetic field. The final mass of product was 2.0 g (12.5 mmol) of Fe_2O_3, and a yield of 68% was calculated.

The nanoparticulated resulting material was characterized by Mössbauer spectroscopy, FT-IR spectroscopy, high-resolution transmission electron microscopy, x-ray powder diffraction, and magnetization measurements and was constituted of stoichiometric maghemite (γ-Fe_2O_3) with a mean diameter (d_{av}) of 11 ± 2 nm (Magro et al., 2012b), which can lead to the formation, upon ultrasound application in water (Falc, model LSB1, 50 kHz, 500 W), of a stable colloidal suspension, without any organic or inorganic coating or derivatization. The surface of these bare maghemite nanoparticles shows peculiar binding properties and can be reversibly derivatized with selected organic molecules. We called these bare nanoparticles surface active maghemite nanoparticles (SAMNs). SAMNs are currently produced and delivered by AINT s.r.l. (Venice, Italy).

2.5. Quantitative determination of curcuminoids by HPLC

The determination of bis-demethoxy-curcumin (BDMC), demethoxy-curcumin (DMC) and curcumin was carried out according to He with modifications (He et al., 1998). A UHPLC system (Ultimate 3000 BioRS, Dionex-Thermo Fisher Scientific Inc., USA) equipped with a diode array detector, was used. An Ace 5 C18 (Advanced Chromatography Technologies, UK) column (5 μm, 25 cm × 4.6 mm) was used for curcuminoids analysis, at 48 °C. The gradient profile of the mobile phase, (A) 0.25% acetic acid in water and (B) acetonitrile (HPLC grade), was as follows: 0–17 min, 40–60% B; 17–32 min, 60–85% B; 32–38 min, 85% B; 38–40 min, 85–40% B; 40–45 min, 40% B; the flow rate was 0.5 mL min^{-1}. The injection volume was 20 μL (full loop). All samples were filtered through 0.22 μm membrane filters before the injection. Curcuminoids were identified by retention times as determined with injections tests with standards (curcumin, demethoxy-curcumin, and bisdemethoxy-curcumin).

2.6. Statistical analysis

The experimental results were expressed as mean values (mean ± SE). Data were analyzed using Sigma Plot (version 10.0) and Assistat statistical program (version 7.7). Significant differences between the samples were evaluated by analysis of variance (ANOVA) followed by Tukey test ($p < 0.05$).

3. Results and discussion

3.1. Effect of plant maturity and light conditions on curcuminoid content in C. longa rhizomes

According to literature, the highest curcuminoid content in *C. longa* rhizome can range from 2.7% to 7.7% with respect to the total dry mass (Nair, 2013). Notwithstanding, the correlation between plant maturity and curcuminoid content is still a matter of debate. Authors found that the highest curcuminoid production was reached in plants between 5 and 9 month growth, while others affirmed that plant maturity does not influence curcumin production (Asghari et al., 2009; Cooray et al., 1988; Manhas and Gill, 2012). Furthermore, other studies, already reporting on the influence of light intensity on productivity and quality of turmeric, indicated a good curcumin productivity in *C. longa* under shading (Bhuiyan et al., 2012; Hossain et al., 2009; Padmapriya et al., 2007; Srikrishnah and Sutharsan, 2015). As the aim of the present study was the optimization of curcuminoid production by *C. longa* rhizomes, as well as of their purification yield, focused to a future application at industrial level, besides curcuminoid content, the limitation of plant biomass represents a crucial aspect for cost reduction of raw material transport, waste generation and solvent volumes in the extraction process. Thus, total curcuminoid content in *C. longa* rhizomes was studied as a function of plant maturity and light conditions specifically in a case study (Sao Paulo state, see Materials and Methods) in the Brazilian agroclimatic zone. Curcuminoid concentration in rhizomes, determined by HPLC in extracts, as a function of days after planting (DAP) and light conditions is reported in Fig. 1. Noteworthy, curcuminoid content, expressed in mg per gram rhizome mass, decreased with time for all tested light conditions. In particular, curcuminoid concentration decreased following an exponential decay, and the corresponding first order kinetic constants were calculated for all the light exposure

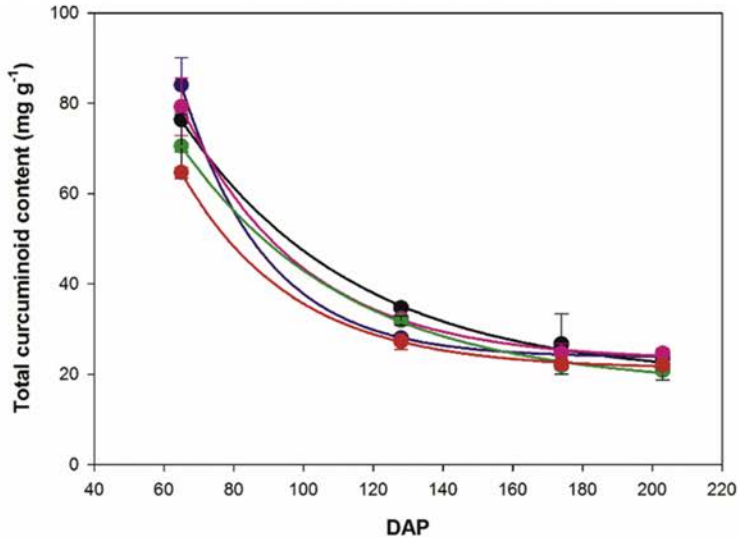

Fig. 1. Curcuminoid content (mg g $^{-1}$) in rhizome mass as a function of *C. longa* maturity (DAP) under different light conditions. Curcuminoid determinations were carried out by HPLC as described in Materials and Methods. Black line = UV exclusion; blue line = 70% shading; pink line = 50% shading; green line = 30% shading; orange line = full sun. Determinations were carried out in triplicate. The maximum error was below 7.0% for all the experimental points. (For interpretation of the references to colour in this figure legend, the reader is referred to the web version of this article.)

conditions. As model, we assumed a single exponential as shown in the following equation:

$$TCC_{(DAP)} = TCC_{maturity} + TCC_0 \times \exp^{(-k \times DAP)}$$

where $TCC_{(DAP)}$ represents the total curcuminoid content (mg g^{-1}) of *Curcuma longa* in a specific day after planting (DAP), $TCC_{maturity}$ is the total curcuminoid content (mg g^{-1}) at the end of the plant growth. TCC_0 is the extrapolated total curcuminoid content at 0 DAP, k is the decay kinetic constant. Interestingly, no significant differences emerged among decay kinetic constants, which were not sensitive on light exposure: the average value resulted $k = 3.0 \pm 0.2 \times 10^{-2}$ days^{-1}. The curcuminoid content reached a plateau after 180 DAP, where it was about 30% with respect to the first determination (65 DAP) (see Fig. 1). Interestingly, at 65 DAP, the influence of light exposure on curcuminoid level was evident. At 65 DAP, curcuminoid content was according to the following order (see Fig. 2): plants under full sun < 30% shading < 50% shading < 70% shading. The exclusion of solar UV radiations resulted in a curcuminoid content comparable to 50% shading. Therefore, the concentration of curcuminoids in rhizomes appears more sensitive to PAR intensity than to UV radiation exclusion (Fig. 2, inset). Furthermore, the dependence of curcuminoid concentration in rhizomes on PAR was well fitted by an exponential curve, characterized by first order constant $k = 3.0 \pm 0.1 \times 10^{-3}$ PAR^{-1}, as shown in the following equation:

$$TCC_{PAR} = TCC_{fs} + TCC_0 \times \exp^{(-k \times PAR)}$$

where TCC_{PAR} represents the total curcuminoid content (mg g^{-1}) of *Curcuma longa* as a function of PAR, TCC_{fs} represents the total curcuminoid content when plants are cultivated under full sun (0% shading), TCC_0 is the extrapolated total curcuminoid content of plants cultivated in the dark (100% shading), and k is decay kinetic constant. The decay led to a minimum curcuminoid concentration value under full sun, at about 1200 PAR (Fig. 2, inset). At this light intensity, the concentration of curcuminoids resulted about 75% with respect to plants grown under 70% shading (Fig. 2, inset). Concluding, according to our results, plants at 65 DAP under 70% shading represents the best conditions for obtaining the highest curcuminoid content in *C. longa* rhizomes (Table 1).

Noteworthy, the biomass produced at 65 DAP is about 7.5% with respect the total biomass produced at the end of growth period (see Table 1). In other words, a potential industrial plant for curcuminoid purification will treat an amount of *C. longa* rhizomes one order of magnitude lower if plants are harvested at 65 DAP, which contain 4 times higher curcuminoid content, than plants at the end of the growth period.

3.2. Binding of curcuminoids to magnetic nanoparticles

Curcuminoids present a keto-enol functionality, which shows strong binding proclivity toward a new category of maghemite nanoparticles, named Surface Active Maghemite Nanoparticles (SAMNs) (Magro et al., 2014b). Curcumin appeared as one of the best ligands for SAMN surface, among an extended list of compounds (Magro et al., 2015c), confirming the literature reporting on the formation of stable complexes between curcumin and iron(III) (Borsari et al., 2002). In the present report, based on preliminary studies (Magro et al., 2015c), an efficient curcuminoid purification process was developed exploiting the influence of solvent polarity on the binding equilibrium. Specifically, *C. longa* rhizomes, collected at 65 DAP, were manually sliced, dried at 65 °C in a ventilated oven and finely ground as described in Methods. Dried and powdered *C. longa* rhizomes were extracted (20 mg mL^{-1}) with 99.6% ethanol. Then, extracts were incubated with stable aqueous colloidal suspensions of SAMNs under magnetic stirring at room temperature for 1 h. Under optimized binding conditions, the aqueous SAMN suspension was added to the ethanol rhizome extract (3:1 v/v), thus, ethanol final concentration was 25%.

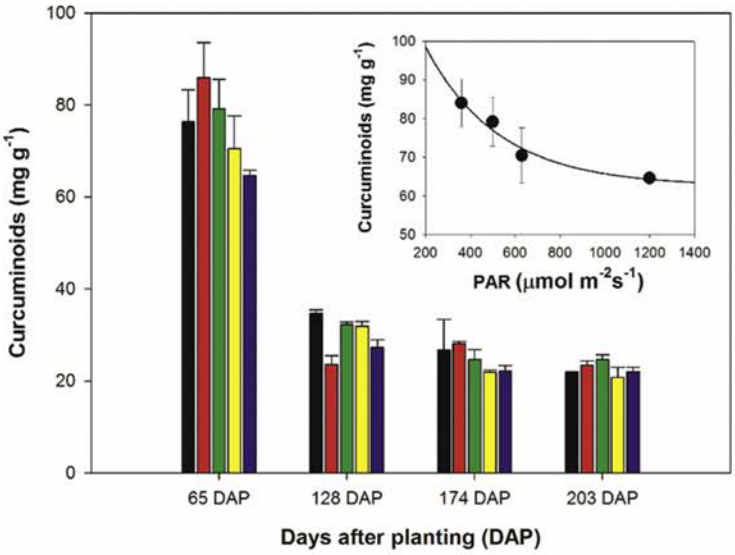

Fig. 2. Curcuminoids content (mg g^{-1}) of *C. longa* cultivated under different light conditions at different DAP. Black bars = UV radiation exclusion; red bars = 70% shading; green bars = 50% shading; yellow bars = 30% shading; blue bars = full sun. **Inset**: Curcuminoid content (mg g^{-1}) in *C. longa* rhizomes at 65 DAP as a function of PAR. The maximum error was below 3.0% for all the experimental points. (For interpretation of the references to colour in this figure legend, the reader is referred to the web version of this article.)

Table 1
Biomass (g) and curcuminoid content (% dry weight) in rhizome of *C. longa* cultivated under 70% shading at different stages of maturity (DAP).

DAP	Rhizome biomass (g)	Curcuminoids (% dry weight)
65	35.6 ± 2.3	8.4 ± 0.6
128	140.2 ± 24.6	2.5 ± 0.1
174	353.3 ± 35.7	2.8 ± 0.1
203	476.8 ± 32.0	2.3 ± 0.1

Values are the mean of six plants and three replicates with standard deviation.

Curcuminoid solubility drastically decreased with the introduction of water, and solvent modification forced the interaction of the biomolecules with nanoparticle surface. Briefly, after the incubation of *C. longa* extracts with SAMNs in 25% of ethanol, a nanobioconjugate (SAMN@curcuminoid) was produced, which was subsequently magnetically isolated and subjected to three washing cycles in water. The possible loss of bound biomolecules from the surface of SAMNs was followed by UV–Vis spectroscopy and resulted below the limit of detection of the instrument (0.25 mg L^{-1} curcuminoid). The chemical interaction between curcuminoids and SAMNs was visually witnessed by a remarkable modification of the color, from brown to red purple, of the SAMN suspension (see Fig. 3, inset).

The SAMN@curcuminoid complex was characterized by UV–Vis spectroscopy confirming the binding of the biomolecules onto the surface exposed iron(III) sites on SAMNs, as already observed in previous papers (Magro et al., 2014b, 2015b). Curcuminoid binding influenced the optical properties of SAMNs as already reported for hybrid nanomaterials, which can display peculiar properties, differently from those inherited from their components. The UV–Vis spectrum of the SAMN@curcuminoid complex was acquired and compared with those of naked SAMNs and of the *C. longa* rhizome extract (see Fig. 3). *C. longa* extract presented an intense yellow color and its spectrum was characterized by an intense band at 430 nm, attributable to the presence of curcuminoids (Rymbai et al., 2011). The electronic absorption spectrum of bare SAMNs, acquired in water, showed a wide band with a maximum at about 400 nm as already reported (Magro et al., 2012a). Conversely, the optical spectrum of the SAMN@curcuminoid complex resulted characterized by the presence of two peaks, at 350 nm and 425 nm (see Fig. 3). Such a dramatic spectral alteration, regarding both the shape and the position of the optical bands, witnessed the occurrence of the binding and provided the evidence of its covalent nature, in agreement with ESR measurement (see hereafter) and with results presented elsewhere (Magro et al., 2014b). It should be mentioned that the SAMN@curcuminoid complex was very stable in water and, if stored at 4 °C, organic molecules remained firmly bound to SAMN surface for at least 12 months.

Transmission electron microscopy (TEM) was used to further characterize the complex between magnetic nanoparticles and curcuminoids (SAMN@curcuminoid). TEM images showed the presence of an organic matrix, forming a shell of about 2.0 nm around iron oxide nanoparticles, characterized by a lower electron density, attributable to curcuminoid molecules layering on the SAMN surface (Fig. 4).

Moreover, the SAMN@curcuminoid complex was characterized by electron spin resonance (ESR) spectroscopy. In particular, ESR spectra of SAMNs and SAMN@curcuminoid were acquired in order to evidence the binding occurrence. As shown in Fig. 5, ESR spectrum of SAMNs, at room temperature, presented a nearly symmetric wide signal characterized by a center field at 2940 Gauss, corresponding to a g factor of 2.39, and a linewidth of 1200 Gauss. Differently, the ESR spectrum of the SAMN@curcuminoid complex was characterized by a center field at 2850 Gauss (g factor of 2.49) and a linewidth of 1140 Gauss. The lower linewidth indicates less magnetic interparticle interactions, and these spectral variations with respect to naked SAMNs suggest a strong binding through electron delocalization over the biomolecule–surface-iron(III)

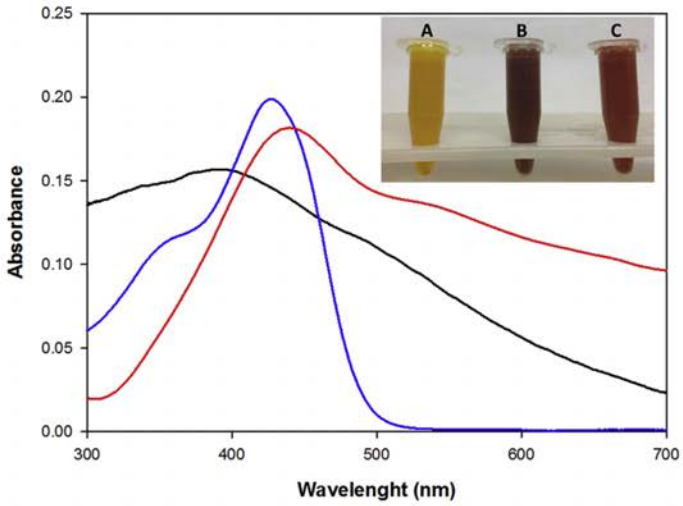

Fig. 3. UV–Vis spectra of naked and curcumin-coated SAMNs (SAMN@curcuminoid) in water. Black, 0.1 g L^{-1} SAMN; Red, 0.1 g L^{-1} SAMN@curcuminoid; Blue, 20 g L^{-1} *C. longa* extract in 25% ethanol. **Inset**. Photographs of materials used for curcumin purification. A) *C. longa* extract (20 g L^{-1}) in 25% ethanol; B) SAMN (0.1 g L^{-1}); C) SAMN@curcuminoid (0.1 g L^{-1}).

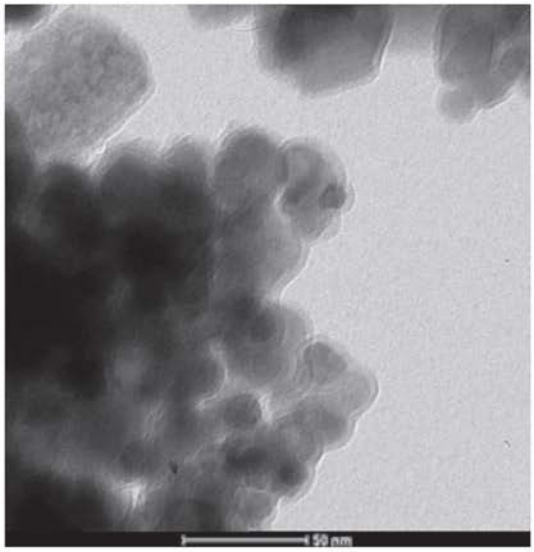

Fig. 4. Transmission electron microscopy image of SAMNs incubated in *C. longa* rhizome extracts.

complex in the SAMN@curcuminoid complex (Amstad et al., 2011).

3.3. Recovery of curcuminoids from the SAMN@curcuminoid complex

The concentration of nanoparticles during the incubation with *C. longa* rhizome extract influenced the fraction of curcuminoids released from the SAMN surface. Thus, curcuminoid binding was tested at SAMN final concentrations in the 1.0–10.0 g L^{-1} range. Interestingly, the highest yield of recovered curcuminoids was obtained with 1.0 g L^{-1} SAMNs. In particular, the fraction of bound curcuminoids, expressed in % with respect to their total amount in the extract, was 93.5% at 1.0 g L^{-1} SAMNs, while at 10.0 g L^{-1} SAMNs was 82.7% (see Table 2). This result was not surprising as at high concentrations (10 g L^{-1}) and in the presence of an organic solvent (ethanol) SAMNs can lead to partial aggregation, lowering the surface area available for binding. Thus, in the present case, the lowest SAMN concentration led to the highest colloidal stability and the highest nanoparticle surface area exposed to the solvent, and available for curcuminoid binding.

The binding process of curcuminoids to SAMN surface was very fast (completed within 5 min) and the resulting nanobioconjugate (SAMN@curcuminoid) was collected by the application of an external magnet. Then, it was extensively washed with water to eliminate loosely bound substances.

The release of curcuminoids from nanoparticle surface, after magnetic purification, was accomplished by incubating the SAMN@curcuminoid complex in 99.6% ethanol. Under these conditions, the release of curcuminoids from the nanobioconjugate was tested with different SAMN concentrations. For example, when the concentration of SAMNs in the *C. longa* rhizome extract was 1.0 g L^{-1} and 10.0 g L^{-1}, the released curcuminoids were 96.0% and 51.2% with respect to the amount of bound biomolecules, respectively (Table 2). Thus, the binding of curcuminoids on 1.0 g L^{-1} SAMNs was completely reversible, and the magnetic nanosystem was able to quantitatively bind and recover the curcuminoid molecules present in the rhizome extracts. For comparison, in a preliminary study, we described the purification of 3.95 mg curcuminoid g^{-1} *C. longa* rhizome by magnetic nanoparticles (Magro et al., 2015c). With respect to this value, in the present protocol the curcuminoid purification protocol was improved up to 69.7 mg curcuminoid g^{-1} *C. longa* rhizome, corresponding to a yield increase of about 17.5 times, using an order of magnitude lower concentration of SAMNs.

The proposed procedure for curcumin purification can be summarized as follows: dried powder of *C. longa* rhizome, collected

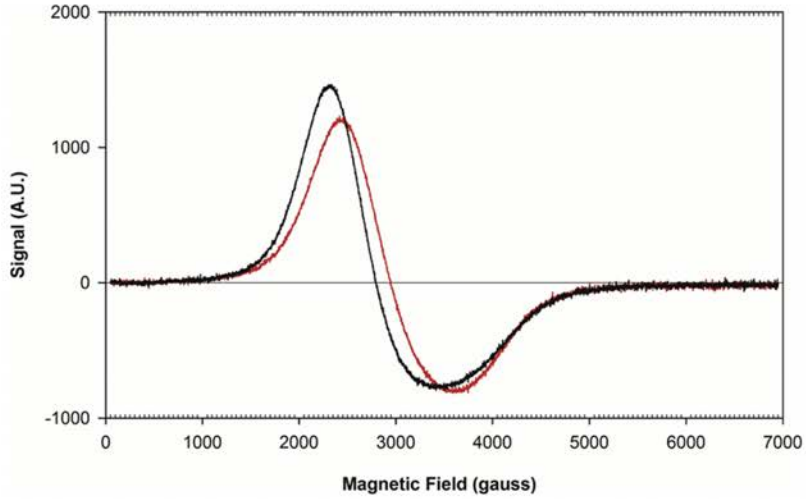

Fig. 5. Electron spin resonance spectra of SAMNs and SAMN@curcuminoid.

Table 2
Curcuminoid binding and release efficiencies in different incubations conditions with SAMNs. Bound curcuminoids were calculated with respect to their total content in the *C. longa* rhizome extracts. Purified curcuminoids were calculated with respect to their amount bound on SAMNs.

EtOH content (%)	Concentration of SAMNs (g L^{-1})	% Bound Curcuminoids	% Purified Curcuminoids
25.0	1	92.6 ± 3.7	95.5 ± 7.8
25.0	10	80.6 ± 13.8	49.9 ± 5.3
99.6	1	9.7 ± 6.1	3.2 ± 3.5
99.6	10	4.9 ± 4.2	13.8 ± 16.0

*Values are the mean and standard deviation of three experiments.

at 65 DAP, was extracted with 99.6% ethanol (1:60 w/v) aided by 5 min sonication (Falc, model LSB1, 50 kHz, 500 W). After decantation (10 min), the supernatant was incubated with SAMNs (1.0 g L^{-1}) for 5 min, under stirring, at room temperature. The nanoparticle containing suspension was subjected to magnetic separation, and the resulting supernatant was eliminated. The collected SAMN@curcuminoid complex was washed with water. The releasing of curcuminoids bound onto the nanoparticles was accomplished by subsequent incubation of SAMN@curcuminoid in 99.6% ethanol (1:60 w/v) for 1 h, at room temperature, and naked nanoparticles were magnetically removed. Under laboratory conditions, the whole process can be accomplished within 80 min. Released curcuminoids in ethanol were dried under low vacuum (100 torr) at 40 °C, leading to 67.4 ± 9.0 mg g^{-1} of a yellow powder, consisting of 47.8 ± 3.8% curcumin, 22.1 ± 2.5% demethoxy-curcumin, and 30.1 ± 3.9% bis-demethoxy-curcumin (by HPLC), with a purity > 98% with respect to the total dry rhizome mass of the extract.

After the curcuminoid purification, and due to the great reversibility of the binding, SAMNs can be recycled and used for other purification processes.

3.4. Pilot plant for curcuminoid purification by magnetic separation

Finally, with the aim of demonstrating the feasibility of the described laboratory approach to be moved to an industrial scale, a prototype plant, consisting of a simple modular and reconfigurable robotic platform, was applied for performing continuous curcuminoid purification, see Fig. 6. It should be mentioned that a modified version of this patented prototype (Magro et al., 2016d) was already described and successfully applied for environmental remediation (Magro et al., 2016e). In the current study, the system was able to process 100 L day^{-1}. Nevertheless, it is readily expandable for larger volumes in an industrial plant (Fig. 6, inset). The proposed prototype comprises two modules (a mixing module and a magnetic separation module), in which the mixing module is a paddle mixer, while the magnetic separation module is an oscillating pan, equipped with a magnetic plate for nanoparticle recovery. The magnetic plate is positioned at the bottom of the pan and the distance between the pan and the plate will vary by pneumatic actuators as the process proceeds (see Fig. 6). The module oscillations and the distance of the magnetic plate are controlled by a software built in-house. Water and SAMNs suspension were moved through the treatment steps by liquid pumps as described (Magro et al., 2016d). Note that all these operations are possible because of the peculiar colloidal stability of SAMNs, their surface reactivity, and the fast binding kinetics. In addition, the synthetic protocol for SAMNs responds to appealing requirements, such as cost effectiveness (below 3 $ g^{-1} at the laboratory scale), environmental sustainability, and industrialization suitability. The synthesis is completely carried out in water, without the necessity of any organic solvent. Moreover, SAMNs do not need any kind of cumbersome, time-consuming, and expensive stabilizing coating, which limits massive applications. Beyond their excellent characteristics in term of binding performances and low environmental impact, SAMNs represent a competitive and sustainable alternative

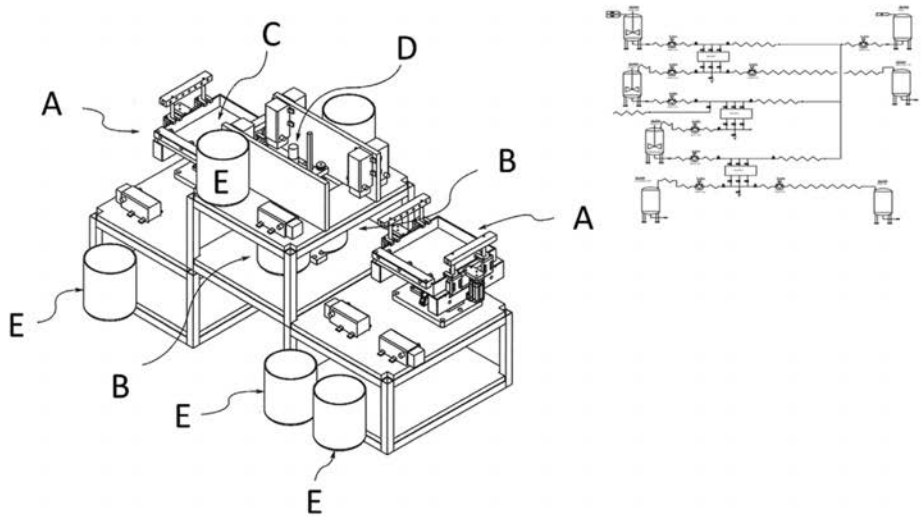

Fig. 6. Schematic representation of the pilot plant used for the recovery of curcuminoids from *C. longa* rhizome extracts by magnetic separation. A: magnetic separation module; B: mixing module; C: separation chamber; D: mixer motor; E: reservoirs for stocking water suspensions of bare SAMNs, ethanolic extract from *C. longa*, water for washing processes, recycled SAMNs, ethanol solution containing purified curcuminoids. **Inset** simplified plant scheme for the treatment of industrial scale volumes of water-ethanol extracts from *C. longa* rhizome.

to standard chromatographic or extraction methods for biomolecule purification.

4. Conclusions

The optimum harvesting time for the maximization of curcuminoid content and the reduction of biomass of *C. longa* in a case study in the Brazilian agro-climatic zone was individuated, as well as the best light exposition condition. The early harvest (65 DAP) led to 4 times higher curcuminoid content per rhizome dry weight than late harvest, reducing biological and chemical wastes as well as plant sizing to 7.5%. Moreover, a new category of maghemite nanoparticles, named Surface Active Maghemite Nanoparticles (SAMNs), was exploited for the magnetic purification of curcuminoids from *C. longa* rhizomes. The proposed magnetic purification protocol led to the recovery of 90% of high purity curcuminoids in a single magnetic purification step. Finally, an automatic modular pilot system for the continuous magnetic separation and purification of curcuminoids was applied, demonstrating the scalability of the presented approach, as SAMNs respond to essential prerequisites of environmental sustainability, and industrialization feasibility.

The reduction of biomass and the consequent waste generation, the minimization of solvent volumes and the costs related to raw material transport, as well as to the high yield and purity of curcuminoids, can be of interest for agro-industries in Brazil.

Acknowledgements

The authors gratefully acknowledge the support by Coordenação de Aperfeiçoamento de Pessoal de Nivel Superior (CAPES – Brazil), process 99999.010436/2014-06, Conselho Nacional de Pesquisa (CNPq – Brazil), process 478372/2013-2 and process 306151/2012-0 and São Paulo Research Fundation (FAPESP - Brazil), process 2013/05644-3 and 2016/22665-2. Moreover, the authors gratefully acknowledge University of Padua (Italy) grant "Assegni di Ricerca Junior" 2014 n. CPDR148959 and CARIPARO Foundation for the support. The authors thank L. Bettinsoli, M. Braga, R. Braga, and A. Gatti for the construction of the pilot plant.

References

Amstad, E., Fischer, H., Gehring, A.U., Textor, M., Reimhult, E., 2011. Magnetic decoupling of surface Fe^{3+} in magnetite nanoparticles upon nitrocatechol-anchored dispersant binding. Chem. Eur. J. 17, 7396–7398.

Asghari, G., Mostajeran, A., Shebli, M., 2009. Curcuminoid and essential oil components of turmeric at different stages of growth cultivated in Iran. Res. Pharm. Sci. 4, 55–61.

Baratella, D., Magro, M., Sinigaglia, G., Zboril, R., Salviulo, G., Vianello, F., 2013. A glucose biosensor based on surface active maghemite nanoparticles. Biosens. Bioelectron. 45, 13–18.

Bhuiyan, M.M.R., Roy, S., Sharma, P.C.D., Rashid, M.H.A., Bala, P., 2012. Impact of multistoreyed agro-forestry systems on growth and yield of turmeric and ginger at Mymensingh, Bangladesh. eSci J. Crop Prod. 1, 19–23.

Bonaiuto, E., Magro, M., Baratella, D., Jakubec, P., Sconcerle, E., Terzo, M., Miotto, G., Macone, A., Agostinelli, E., Fasolato, S., Venerando, R., Salviulo, G., Malina, O., Zboril, R., Vianello, F., 2016. Ternary hybrid γ-Fe_2O_3/Cr^{VI}/Amine Oxidase nanostructure for electrochemical sensing: application for polyamine detection in tumor tissue. Chem. Eur. J. 22, 6846–6852.

Borsari, M., Ferrari, E., Grandi, R., Saladini, M., 2002. Curcuminoids as potential new iron-chelating agents: spectroscopic, polarographic and potentiometric study on their Fe(III) complexing ability. Inorg. Chim. Acta 328, 61–68.

Camargo, N.M., Klamt, E., Kauffman, J.H., 1987. Classificação de solos usada em levantamentos pedológicos no Brasil. Bol. Soc. Bras. Ciência do Solo 12, 11–33.

Cmiel, V., Skopalik, J., Polakova, K., Solar, J., Havrdova, M., Milde, D., Justan, I., Magro, M., Starcuk, Z., Provaznik, I., 2016. Rhodamine bound maghemite as a long-term dual imaging nanoprobe of adipose tissue-derived mesenchymal stromal cells. Eur. Biophys. J. http://dx.doi.org/10.1007/s00249-016-1187-1.

Cooray, N.F., Jansz, E., Ranatunga, J., Wimalasena, S., 1988. Effect of maturity on some chemical constituents of turmeric (Curcuma longa L.). J. Nat. Sci. Found. Sri Lanka 16, 39–51.

Gupta, S.C., Kismali, G., Aggarwal, B.B., 2013. Curcumin, a component of turmeric: from farm to pharmacy. BioFactors 39, 2–13.

He, X.-G., Lin, L.-Z., Lian, L.-Z., Lindenmaier, M., 1998. Liquid chromatography–electrospray mass spectrometric analysis of curcuminoids and sesquiterpenoids in turmeric (Curcuma longa). J. Chromatogr. A 818, 127–132.

Hossain, M.A., Akamine, H., Ishimine, Y., Teruya, R., Aniya, Y., Yamawaki, K., 2009. Effects of relative light intensity on the growth, yield and curcumin content of turmeric (Curcuma longa L.) in Okinawa, Japan. Plant Prod. Sci. 12, 29–36.

Kitts, D., Weiler, K., 2003. Bioactive proteins and peptides from food sources. Applications of bioprocesses used in isolation and recovery. Curr. Pharm. Des. 9,

1309–1323.
Kulkarni, S.J., Maske, K.N., Budre, M.P., Mahajan, R.P., 2012. Extraction and purification of curcuminoids from Turmeric (Curcuma longa L.). Int. J. Pharmacol. Pharm. Technol. 1, 81–84.
Magro, M., Faralli, A., Baratella, D., Bertipaglia, I., Giannetti, S., Salviulo, G., Zboril, R., Vianello, F., 2012a. Avidin functionalized maghemite nanoparticles and their application for recombinant human biotinyl-SERCA purification. Langmuir 28, 15392–15401.
Magro, M., Sinigaglia, G., Nodari, L., Tucek, J., Polakova, K., Marusak, Z., Cardillo, S., Salviulo, G., Russo, U., Stevanato, R., Zboril, R., Vianello, F., 2012b. Charge binding of rhodamine derivative to OH^- stabilized nanomaghemite: universal nanocarrier for construction of magnetofluorescent biosensors. Acta Biomater. 8, 2068–2076.
Magro, M., Baratella, D., Pianca, N., Toninello, A., Grancara, S., Zboril, R., Vianello, F., 2013. Electrochemical determination of hydrogen peroxide production by isolated mitochondria: a novel nanocomposite carbon-maghemite nanoparticle electrode. Sens. Actuators B Chem. 176, 315–322.
Magro, M., Baratella, D., Salviulo, G., Polakova, K., Zoppellaro, G., Tucek, J., Kaslik, J., Zboril, R., Vianello, F., 2014a. Core-shell hybrid nanomaterial based on prussian blue and surface active maghemite nanoparticles as stable electrocatalyst. Biosens. Bioelectron. 52, 159–165.
Magro, M., Campos, R., Baratella, D., Lima, G., Holà, K., Divoky, C., Stollberger, R., Malina, O., Aparicio, C., Zoppellaro, G., Zboril, R., Vianello, F., 2014b. A magnetically drivable nanovehicle for curcumin with antioxidant capacity and MRI relaxation properties. Chem. Eur. J. 20, 11913–11920.
Magro, M, Valle, G., Russo, U., Nodari, L., Vianello, F., 2015a. Maghemite nanoparticles and method for preparing thereof. Patent number US Patent 8,980,218, 2015; EP 2 596 506 B1 2014.
Magro, M., Baratella, D., Jakubec, P., Zoppellaro, G., Tucek, J., Aparicio, C., Venerando, R., Sartori, G., Francescato, F., Mion, F., Gabellini, N., Zboril, R., Vianello, F., 2015b. Triggering mechanism for DNA electrical conductivity: reversible electron transfer between DNA and iron oxide nanoparticles. Adv. Funct. Mater 25, 1822–1831.
Magro, M., Campos, R., Baratella, D., Ferreira, M.I., Bonaiuto, E., Corraducci, V., Uliana, M.R., Lima, G.P.P., Santagata, S., Sambo, P., Vianello, F., 2015c. Magnetic purification of curcumin from Curcuma longa rhizome by novel naked maghemite nanoparticles. J. Agric.Agric. Food Chem. 63, 912–920.
Magro, M., Bonaiuto, E., Baratella, D., de Almeida Roger, J., Jakubec, P., Corraducci, V., Tuček, J., Malina, O., Zbořil, R., Vianello, F., 2016a. Electrocatalytic nanostructured ferric tannates: characterization and application of a polyphenol nanosensor. ChemPhysChem 17, 3196–3203.
Magro, M., Moritz, D.E., Bonaiuto, E., Baratella, D., Terzo, M., Jakubec, P., Malina, O., Cepe, K., De Aragao, G.M.F., Zboril, R., Vianello, F., 2016b. Citrinin mycotoxin recognition and removal by naked magnetic nanoparticles. Food Chem. 203, 505–512.
Magro, M., Fasolato, L., Bonaiuto, E., Andreani, N.A., Baratella, D., Corraducci, V., Miotto, G., Cardazzo, B., Vianello, F., 2016c. Enlightening mineral iron sensing in Pseudomonas fluorescens by surface active maghemite nanoparticles: involvement of the OprF porin. Biochim. Biophys. Acta 1860, 2202–2210.
Magro, M., Bettinsoli, L., Braga, M., Braga, R., Gatti, A., Vianello, F., 2016d. Apparatus and method for a separation through magnetic nanoparticles. Patent number WO 016/157027 A1.
Magro, M., Domeneghetti, S., Baratella, D., Jakubec, P., Salviulo, G., Bonaiuto, E., Venier, P., Malina, O., Tuček, J., Ranc, V., Zoppellaro, G., Zbořil, R., Vianello, F., 2016e. Colloidal Surface Active Maghemite Nanoparticles for biologically safe Cr^{VI} remediation: from core-shell nanostructures to pilot plant development. Chem. Eur. J. 22, 14219–14226.
Manhas, S.S., Gill, B.S., 2012. Effect of different cultural practices on production of turmeric (Curcuma longa L.) in Punjab. J. Spic. Arom. Crops 21, 53–58.
Miotto, G., Magro, M., Terzo, M., Zaccarin, M., Da Dalt, L., Bonaiuto, E., Baratella, D., Gabai, G., Vianello, F., 2016. Protein corona as a proteome fingerprint: the example of hidden biomarkers for cow mastitis. Colloids Surf. B 140, 40–49.
Nair, K.P.P., 2013. The botany of turmeric. In: Nair, K.P.P. (Ed.), The Agronomy and Economy of Turmeric and Ginger: the Invaluable Medicinal Spice Crops. Elsevier Scientific Publishing Company, Amsterdam, pp. 7–32.
Padmapriya, S., Chezhiyan, N., Sathiyamurthy, V.A., 2007. Effect of shade and integrated nutrient management on biochemical constituents of turmeric (Curcuma longa L.). J. Hortic. Sci. 2, 123–129.
Rymbai, H., Sharma, R.R., Srivastav, M., 2011. Biocolorants and its implications in health and food industry-a review. Int. J. PharmTech Res. 3, 2228–2244.
Santos, H.G., Jacomine, P.K.T., Anjos, L.H.C., Oliveira, V.A., Oliveira, J.B., Coelho, M.R., Lumbreras, J.F., 2006. Sistema brasileiro de classificação de solos, second ed. Embrapa solos, Rio de Janeiro.
Sinigaglia, G., Magro, M., Miotto, G., Cardillo, S., Agostinelli, E., Zboril, R., Bidollari, E., Vianello, F., 2012. Catalytically active bovine serum amine oxidase bound to fluorescent and magnetically drivable nanoparticles. Int. J. Nanomed 7, 2249–2259.
Skopalik, J., Polakova, K., Havrdova, M., Justan, I., Magro, M., Milde, D., Knopfova, L., Smarda, J., Polakova, H., Gabrielova, E., Vianello, F., Michalek, J., Zboril, R., 2014. Mesenchymal stromal cell labeling by new uncoated superparamagnetic maghemite nanoparticles in comparison with commercial Resovist – an initial in vitro study. Int. J. Nanomed 9, 5355–5372.
Srikrishnah, S., Sutharsan, S., 2015. Effect of different shade levels on growth and tuber yield of turmeric (Curcuma longa L.) in the Batticaloa District of Sri Lanka. Am. Euras. J. Agric.Agric. Environ. Sci. 15, 813–816.
Turková, J., 1978. Affinity Chromatography, first ed. Elsevier Scientific Publishing Company, Amsterdam.
Urbanova, V., Magro, M., Gedanken, A., Baratella, D., Vianello, F., Zboril, R., 2014. Nanocrystalline iron oxides, composites, and related materials as a platform for electrochemical, magnetic, and chemical biosensors. Chem. Mater 26, 6653–6673.
Venerando, R., Miotto, G., Magro, M., Dallan, M., Baratella, D., Bonaiuto, E., Zboril, R., Vianello, F., 2013. Magnetic nanoparticles with covalently bound self-assembled protein corona for advanced biomedical applications. J. Phys. Chem. C 117, 20320–20331.

7.2- Characterization of the structure and electrochemical properties of the nanostructured SAMN@TA and determination of polyphenols in real samples.

Publication number 2:

Magro, M. Bonaiuto, E Baratella, D. **de Almeida Roger, J**. Jakubec, P. Corraducci, V. Tucek, J. Malina, O. Zboril, R., Vianello, F. 2016. Electrocatalytic Nanostructured Ferric Tannates: Characterization and Application of a Polyphenol Nanosensor. 2016. ChemPhysChem. 17, 3196 – 3203.

ChemPubSoc Europe

DOI: 10.1002/cphc.201600718

CHEMPHYSCHEM Articles

Electrocatalytic Nanostructured Ferric Tannates: Characterization and Application of a Polyphenol Nanosensor

Massimiliano Magro,[a] Emanuela Bonaiuto,[a] Davide Baratella,[a] Jessica de Almeida Roger,[a] Petr Jakubec,[b] Vittorino Corraducci,[a] Jiri Tuček,[b] Ondrej Malina,[b] Radek Zbořil,[b] and Fabio Vianello*[a, b]

A novel core–shell hybrid nanomaterial composed of peculiar maghemite nanoparticles (surface-active maghemite nanoparticles (SAMNs)) as the core and tannic acid (TA) as the shell was developed by self-assembly of ferric tannates onto the surface of SAMNs by simple incubation in water. The hybrid nanomaterial (SAMN@TA) was characterized by using UV/Vis, FTIR, and Mössbauer spectroscopies, magnetization measurements, and X-ray powder diffraction, which provide evidence of a drastic reorganization of the iron oxide surface upon reaction with TA and the formation of an outer shell that consists of a cross-linked network of ferric tannates. According to a Langmuir isotherm analysis, SAMN@TA offers one of most stable iron complexes of TA reported in the literature to date. Moreover, SAMN@TA was characterized by using electrical impedance spectroscopy, voltammetry, and chronoamperometry. The nanostructured ferric tannate interface showed improved conductivity and selective electrocatalytic activity toward the oxidation of polyphenols. Finally, a carbon-paste electrode modified with SAMN@TA was used for the determination of polyphenols in blueberry extracts by square-wave voltammetry.

1. Introduction

Hybrid nanomaterials, composed of different functional components and different nanoscale functionalities, have attracted increasing interest from materials scientists due to their combined physicochemical properties and great potential applications in the areas of electronics,[1] photonics,[2] biotechnology,[3] biosensing,[4] nanotechnology,[5,6] and catalysis.[7,8] Of the hybrid nanoparticle families, magnetic iron oxide nanoparticles play an important role in a wide range of disciplines, such as magnetic fluids,[9] environmental remediation,[10] magnetic energy storage,[11] and electrochemical sensing platforms.[12–14] Moreover, iron oxide nanoparticles have been studied and used in fields such as drug delivery systems,[15] tissue repair,[16] and magnetic resonance imaging (MRI).[17]

Nanotechnological applications of iron oxides involve two crystal forms, namely magnetite (Fe_3O_4) and maghemite (γ-Fe_2O_3) and, to the best of our knowledge, to date only magnetite has been explored for the development of hybrids with tannic acid.[18–22]

[a] Dr. M. Magro, Dr. E. Bonaiuto, Dr. D. Baratella, Dr. J. de Almeida Roger, V. Corraducci, Prof. F. Vianello
Department of Comparative Biomedicine and Food Science
University of Padua
Agripolis, Viale dell'Università 16, Legnaro, 35020 PD (Italy)
E-mail: fabio.vianello@unipd.it

[b] Dr. P. Jakubec, Dr. J. Tuček, Dr. O. Malina, Prof. R. Zbořil, Prof. F. Vianello
Regional Centre for Advanced Technologies and Materials
Palacky University
17. listopadu 1192/12, 771 46, Olomouc (Czech Republic)

Supporting Information for this article can be found under http://dx.doi.org/10.1002/cphc.201600718.

Recently, we developed a novel wet synthetic pathway for producing a new type of superparamagnetic nanoparticle that consists of maghemite (γ-Fe_2O_3) that reveals peculiar surface characteristics, excellent colloidal stability, reversible direct binding of organic molecules without the need for any additional organic or inorganic surface modification, unique spectroscopic properties, and well-defined crystalline structure.[23,24] We called these nanoparticles surface-active maghemite nanoparticles (SAMN). This nanomaterial was characterized by using bulk techniques, such as in-field Mössbauer spectroscopy, magnetization measurements, X-ray powder diffraction, and FTIR spectroscopy. The most prominent peculiarity of these nanoparticles is the ability to form stable colloidal suspensions in water without any organic or inorganic coating to prevent their aggregation and, at the same time, they are able to bind specific organic molecules, which leads to composite materials that can be exploited for biotechnological applications.[25–27]

Herein, we prepared and characterized a novel hybrid by coating SAMNs with tannins. Tannins are usually classified into two groups: proanthocyanidins and hydrolyzable tannins. Proanthocyanidins are flavonoid oligomers of catechin and epicatechin and their gallic acid esters. Hydrolysable tannins are composed of gallic and ellagic acid esters of core molecules that consist of polyols, such as sugars, and phenolics, such as catechin. Tannic acid (P-penta-*O*-galloyl-D-glucose) is the model compound for this group of tannins,[28,29] and we used this substance for SAMN modification.

Tannins interact with several iron oxide crystalline forms, such as lepidocrocite (γ-FeOOH), goethite (α-FeOOH), magnet-

ite (Fe_3O_4), and maghemite (γ-Fe_2O_3).[7,30–34] TA easily complexes Fe^{3+} ions to form complexes of known low solubility in water.[35] In fact, precipitated ferric tannates form a protective layer with corrosion-inhibiting properties on steel.[36]

Herein, we present an optimized procedure for the preparation of a nanostructured SAMN–TA hybrid (SAMN@TA). The resulting SAMN@TA complex was extremely stable and was structurally and electrochemically characterized. The reaction between SAMNs and TA led to a drastic modification of the nanoparticle surface and a change in the SAMN properties. The core–shell nanostructure was successfully applied for the development of an electrochemical application for the detection of polyphenol content in blueberries by using square-wave voltammetry. To the best of our knowledge, this study represents the first example of the electrocatalysis of ferric tannates at the interface of iron oxide nanoparticles.

2. Results and Discussion

2.1. Development of a Nanostructured Ferric Tannate Interface on SAMNs

The optical spectrum of TA was acquired in 50 mM tetramethylammonium perchlorate, pH 7.0, and exhibited two absorbance peaks at $\lambda = 211$ and 279 nm (see Figure S1 in the Supporting Information). For the determination of TA concentration, a calibration curve was built by using a molar extinction coefficient of $38.5 \times 10^3\ M^{-1}\,cm^{-1}$ at $\lambda = 279$ nm, which was comparable to data reported for other aqueous buffers.[37]

TA is a known chelator of iron(III) due to the combined action and the vicinity of hydroxyl groups on the aromatic rings.[38] The binding of TA on SAMNs can be explained by considering the peculiar surface chemistry of the nanomaterial, and in particular by taking into account the availability and reactivity of the previously demonstrated presence of under-coordinated iron(III) sites on the surface of these nanoparticles.[39]

The binding process of TA (20 μM) on the SAMN surface (0.1, 0.2, 0.5, 1.0, 1.5, 2.0 $g\,L^{-1}$) was monitored in 50 mM tetramethylammonium perchlorate, pH 7.0. The amount of TA bound on the SAMN surface was estimated by determining the free TA in solution after binding by using spectrophotometry at $\lambda = 279$ nm (Figure 1).

As shown in Figure 1, the TA concentration in solution decreased as a function of SAMN concentration, which demonstrates the ability of SAMNs to sequestrate TA. In particular, free TA was completely sequestered (>98%) at 0.5 $g\,L^{-1}$ SAMN. The mass of TA on iron oxide nanoparticles in the SAMN@TA complex was calculated and was found to be 68.0 $mg\,g^{-1}$ SAMNs. It should be noted that this value does not represent the ligand concentration at saturation on the surface (see below).

The proclivity of different components to join reversibly into a complex is generally expressed in term of stability constants. Usually, nanomaterial binding properties are compared based on their maximum adsorption capacities, that is, their maximum loading.

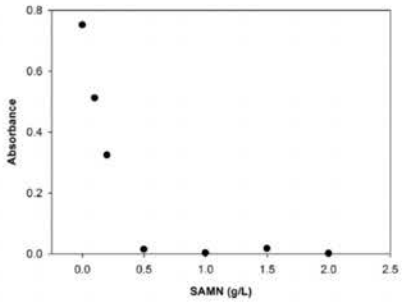

Figure 1. Sequestration of tannic acid by SAMNs, studied by using spectrophotometry at $\lambda = 279$ nm. Measurements were carried out in 0.1 $mol\,L^{-1}$ PBS, pH 7.0, in the presence of 20 μM tannic acid.

TA binding on SAMNs was analyzed according to the Langmuir isotherm model.[40,41] For example, an experiment was performed with TA in the 5 to 100 μM concentration range, with SAMN at a constant concentration of 0.5 $g\,L^{-1}$ (Figure S2). The nanoparticle surface fractional coverage was calculated by using the following saturation function:[42,43]

$$\theta = \frac{\Gamma}{\Gamma_{max}} = \frac{K\,[TA]}{1 + K[TA]}$$

in which θ is the surface fractional coverage of bound substance, Γ_{max} is the surface concentration of TA at full coverage, K is the apparent stability constant, and Γ is the surface concentration of associated TA when its bulk concentration is [TA]. A linear plot of the experimentally determined $\theta - 1$ value as a function of [TA]-1 gives the value of the binding constant, K. In the case of the SAMN@TA complex, K was 911.0 $mL\,mg^{-1}$ and Γ_{max} was 161.3 $mg\,g^{-1}$. Taking into account the TA molar mass (see the Experimental Section) and the SAMN surface area (46.23 $m^2\,g^{-1}$), determined by using the BET method, the amount of polyphenol on the metal oxide surface was estimated to be about 1.2 TA molecules per nm^2.

The binding of TA on solid materials is an object of interest in the field of environmental remediation, as it is commonly considered as a pollutant, and various nanomaterials have been proposed for its removal.[20,44–47] Within this context, the absorption efficiency of SAMNs toward TA stands out as one of the most competitive (Table 1). The observed high binding constant can be explained by the characterization of the SAMN@TA complex (see below), which indicated the occurrence of dramatic structural changes in the maghemite nanoparticle surface that revealed the irreversibility of the binding and, as a consequence, the stability of the self-assembled TA shell. Moreover, experiments were carried out to test the release of TA from the SAMN surface to provide a deeper insight into the TA–SAMN interaction and to test the stability of the complex. Compared with other previously studied SAMN surface modifiers, absolute ethanol and 0.5 M NH_4OH, which represent the two main releasing conditions for SAMN complexes, were unsuccessful. Accordingly, of the substances tested for

Table 1. Comparison of stability constants (K) and loading capacity (Γ_{max}) obtained by using a Langmuir isotherm analysis of nanomaterials reported in the literature.

Material	K [mL mg^{-1}]	Γ_{max} [mg g^{-1}]	Ref.
chitosan-coated attapulgite	154	95.2	[44]
magnetic basic anion exchange resin (MAEX)	109	192.1	[45]
magnetic lignocellulosic adsorbent	35	112.4	[46]
amino-functionalized magnetic nanoadsorbent (Fe_3O_4@SiO_2-NH_2)	200	140.8	[20]
cetylpyridinium bromide modified zeolites	918	111.0	[47]
SAMNs	911	161.3	this work

binding on SAMNs,[48,49] TA binding stands out by showing one of the highest Langmuir stability constants (K = 911.0 mL mg^{-1}), comparable to genomic DNA, which gives irreversible complexes with SAMNs.[39]

2.2. Characterization of the SAMN@TA Complex by Using Optical and IR Spectroscopy

The SAMN@TA complex was magnetically isolated and washed several times with water. The complex was stable, without any loss of TA into solution, as verified by spectrophotometry.

The IR spectrum (FTIR spectroscopy) of the as-prepared SAMN@TA complex is shown in Figure 2A and compared with the FTIR spectrum of TA only; all major spectral bands of the TA spectrum are reflected in the FTIR spectrum of the hybrid nanomaterial. The spectral bands at 1016, 1081, and 1179 cm^{-1} can be interpreted as vibrations of C–O groups in the TA structure. Bands at 1308 and 1443 cm^{-1} originate from a bending of aromatic carbons. The bands of TA bound on SAMNs are spectrally shifted towards higher wavenumbers, with a spectral shift approximately of 50 cm^{-1}. This shift can be interpreted as a result of the interaction of TA with the nanoparticle surfaces.

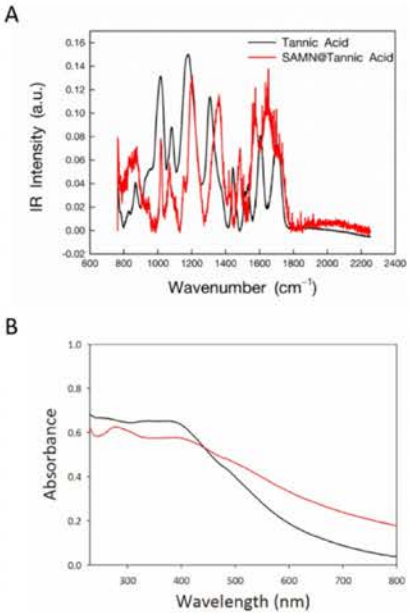

Figure 2. Spectroscopic characterization of the as-prepared SAMN@TA complex. A) FTIR spectra of tannic acid (black) and the SAMN@TA complex (red). B) Optical spectra of bare SAMNs (40 μg mL^{-1}, black) and SAMN@TA (40 μg mL^{-1}, red) in tetramethylammonium perchlorate (50 mmol L^{-1}), pH 7.0.

The SAMN@TA complex was further characterized by using optical spectroscopy and Figure 2B shows the spectra of bare SAMNs and SAMN@TA. It should be noted that optical spectroscopy has already been used to investigate reorganization of the maghemite nanoparticle surface in the presence of several modifiers.[23,25–27,39,48] The electronic absorption spectrum of bare SAMNs shows a wide band with a maximum at about λ = 400 nm (Figure 2B), characterized by an extinction coefficient of 1520 M^{-1} cm^{-1}, expressed as the Fe_2O_3 molar concentration. Note that SAMN@TA shows a wide absorption band characterized by a maximum of absorption at λ = 420 nm and a shoulder at λ = 490 nm (Figure 2B). Furthermore, a peak at about λ = 280 nm is observed and attributed to the aromatic rings of TA (see Figure S1 for comparison). The spectral modifications of SAMNs upon TA binding and the redshift in the λ = 400 nm band revealed the chelation of TA on the iron(III) sites at the interface with SAMNs.

According to the surface reconstruction theory, the modification of optical properties of nanocrystalline metal oxide occurs as a consequence of ligand binding.[39,50] In fact, in the SAMN size domain, the surface atoms adjust their coordination environment to form under-coordinated metal sites. Thus, ligand binding is favored because ligand adsorption induces the restoration of dangling bonds on the nanoparticle surface. Fundamental prerequisites of the theory are colloidal stability, high crystallinity, dimensions below 20 nm, and a proclivity to adsorb chelating ligands. Therefore, this approach can be effectively used on SAMNs and the observed optical features can be explained in term of restructuration of SAMN surface by TA.

2.3. Structural and Morphological Characterization of SAMN@TA

The magnetic properties of the SAMN@TA complex were examined. In Figure 3a, b, the magnetization versus an external magnetic field (hysteresis loops) and magnetization versus temperature (ZFC/FC) curves are presented. The hysteresis loop measured at 5 K (Figure 3a) reveals a symmetric homogeneous profile around the origin, with the significant values of coercivity (24.06 mT) and remanence (14.29 Am^2 kg^{-1}). These values are in good agreement with those reported for the γ-Fe_2O_3 nanoparticulate system.[23] Conversely, the saturation magnetization (46.98 Am^2 kg^{-1}) was significantly decreased on binding with TA, and a dramatic decrease of about 40% with respect to the parent maghemite was observed

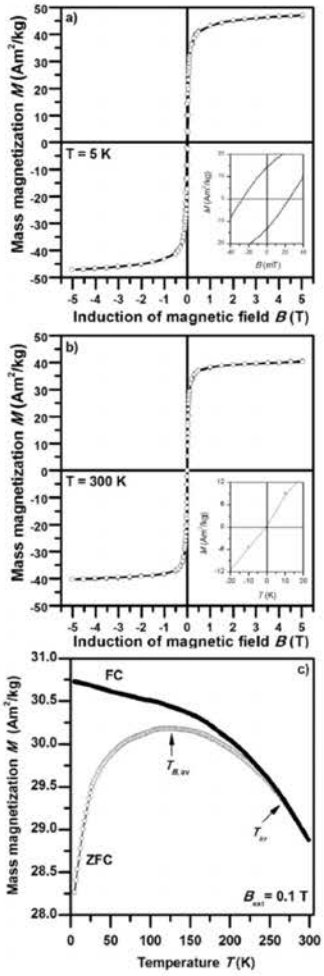

Figure 3. Hysteresis loops of the SAMN@TA complex measured at a) 5 and b) 300 K. Insets: Magnification of the magnetic field (M) in the low-field region. c) ZFC/FC magnetization curves measured for the SAMN@TA complex under an external magnetic field of 0.1 T.

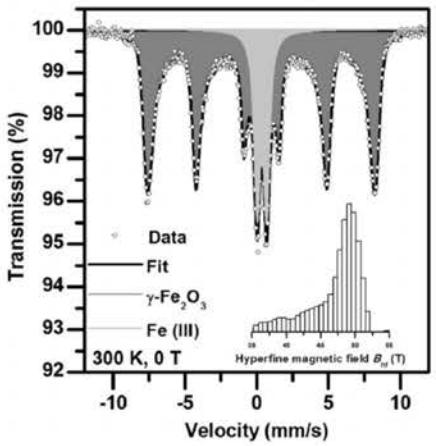

Figure 4. ^{57}Fe Mössbauer spectrum of a) bare SAMNs and b) SAMN@TA complex recorded at room temperature and without an external magnetic field.

(≈77 Am² kg^{-1}).[24] This alteration is due to the presence of a diamagnetic phase, very likely the TA shell, on the surface of maghemite nanoparticles (Table S1, and below). The effect of a diamagnetic substance is also manifested by the nonsaturated curve even at a high magnetic field (5 T). The magnetization versus external magnetic field measurement recorded at room temperature does not show any sign of hysteresis (see Figure 3b). The profile of nonhysteresis behavior is a consequence of the superspins of all magnetic nanoparticles, which fluctuate between the orientations of the easy axis of magnetization. This suggests that the system behaves in a superparamagnetic manner. To confirm this superparamagnetic behavior, ZFC/FC magnetization measurements were carried out (Figure 3c). The broad maximum on the ZFC curve (around 127 K) confirms the freezing of the spins to the magnetically blocked regime, and below this temperature the system is in a completely magnetically blocked state. The maximum at the ZFC curve corresponds to the average blocking temperature ($T_{B,av}$) of nanoparticles with the most probable size in the assembly. No change in the slope of the FC magnetization curve, even below T_B, is evidence of the weak magnetic interactions between all magnetic nanoparticles, most probably based on dipole–dipole interactions. The separation of two curves in the ZFC/FC measurement is known as the temperature of irreversibility (T_{irr}), which marks the onset of the blocking mechanism that belongs to the largest nanoparticles in the system. In the SAMN@TA system T_{irr} is around 270 K, which is far from the values of T_B, which suggests a broad particle-size distribution.

To provide deeper insight into the chemical nature, structural, and magnetic properties of the iron oxide phase, zero-field ^{57}Fe Mössbauer spectroscopy was used. The Mössbauer spectra of the SAMN and SAMN@TA samples are shown in Figure 4, and the values of the Mössbauer hyperfine parameters, derived from the spectrum fitting, are listed in Table S2. At room temperature, the Mössbauer spectrum of the SAMN sample features only one sextet with non-Lorentzian line profiles. The isomer shift (≈0.31 mm s^{-1}), quadrupole splitting (≈0.00 mm s^{-1}), and hyperfine magnetic field (≈46.1 T) values were characteristics of γ-Fe_2O_3.[23] The distribution of the hyperfine magnetic field was used to account for collective magnetic excitations, a phenomenon that typically emerges in nanoparticle systems if a nanoparticle superspin fluctuates/rotates around the easy axis of magnetization established by nanoparticle magnetic anisotropy.

The presence of collective magnetic excitations presages the passage from a magnetically ordered state to a superparamag-

netic regime. However, no doublet is observed, which implies that all the γ-Fe_2O_3 nanoparticles are still in the magnetically blocked state in the time window of the Mössbauer technique ($\approx 10^{-8}$ s). More importantly, in addition to the sextet assigned to γ-Fe_2O_3, the room-temperature ^{57}Fe Mössbauer spectrum of the SAMN@TA sample shows a doublet with an isomer shift (≈ 0.35 mm s^{-1}) and a quadrupole splitting (≈ 0.72 mm s^{-1}) typical for Fe^{III} molecular species; from the spectral area, the doublet accounts for approximately 20% of the total iron(III) content in the sample.

It should be taken into account that TA reacts with Fe^{3+} ions to produce complexes of known low solubility in water, which leads to the formation of stable protective coatings on weathered steel and iron surfaces.[36] This impressive presence of Fe^{3+} ions in SAMN@TA samples shows the conversion of 20% of the γ-Fe_2O_3 iron oxide into TA–Fe^{3+} complexes. Considering the γ-Fe_2O_3 molar mass (160 g mol^{-1}) and SAMN surface area (46.23 m^2 g^{-1}), as determined by using the BET method, it was possible to calculate the number of Fe^{3+} atoms in the parent metal oxide surface that were involved in the shell formation. We estimated that about 32.6 Fe^{3+} atoms per nm^2 of the SAMN surface reacted with TA. Furthermore, based on Mössbauer spectroscopy measurements and a Langmuir isotherm study, we calculated that the shell of SAMN@TA is characterized by about 26.5 Fe^{3+} ions for each TA molecule. Therefore, Mössbauer spectroscopy and magnetization measurements are fully in harmony with the Langmuir isotherm study. In fact, magnetization measurements, which revealed the presence of an organic coating, showed a 40% loss in magnetic saturation. In an acceptable approximation, this value can be likely interpreted as the sum of the degraded paramagnetic γ-Fe_2O_3 (20%) and the TA shell (11%), calculated according to the Langmuir isotherm, and accounting for the reaction of TA molecules with Fe^{3+} on the SAMN surface to form a ferric tannate.[38]

High-resolution TEM images of the SAMN@TA complex were acquired (see Figure 5), and revealed the formation of core–shell hybrid nanostructures. Note that a ferric tannate network on the SAMN surface characterized by a lower electron density is observable, in comparison with the metal oxide core.

The SAMN@TA complex was further characterized by using X-ray powder diffraction (XRPD). The diffraction pattern is presented in Figure S3. Three crystalline phases were identified by using XRPD analysis: a major phase (93% w/w) was identified as maghemite (i.e. γ-Fe_2O_3) in the cubic structure (space group *P*4332) with a lattice parameter of 0.8342 nm and a mean X-ray coherence length (MCL) of 22 nm; the minor phases were found to be hematite (α-Fe_2O_3, 5% w/w) and lepidocrocite (γ-FeOOH, 2% w/w). All parameters derived by using a Rietveld refinement are summarized in Table S3.

According to the literature,[51] it has been shown that tannins are able to react with iron to form insoluble amorphous compounds of mono- and bis-type tannate complexes, for example, bis-ferric tannate. According to the Mössbauer and XRPD results, Fe^{3+} ions can be considered the most important precursors for the formation of ferric tannate complexes on the surface of SAMNs.

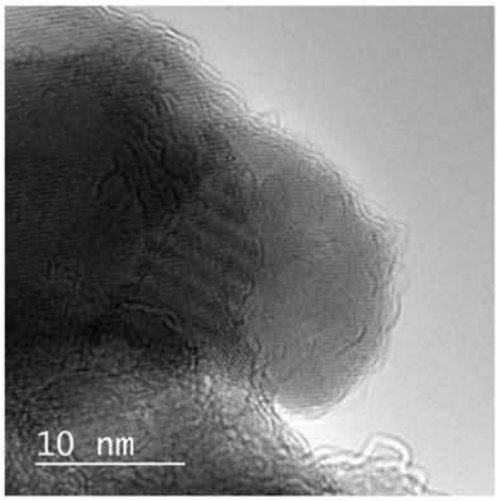

Figure 5. High-resolution transmission electron microscopy (HR-TEM) image of the SAMN@TA complex.

2.4. Electrochemical Characterization of SAMN@TA

The novel nanostructured ferric tannate on the SAMN surface was characterized by using electrochemical techniques because the electrocatalytic properties of bare SAMNs have already been studied and applied.[52,53]

The SAMN@TA complex was inserted in a carbon-paste electrode (CPE) and characterized by using cyclic voltammetry and chronoamperometry. The cyclic voltammograms of CPE modified with TA (1% w/w), SAMNs, and SAMN@TA (15% w/w), in the absence of any electroactive substance, are reported for comparison in Figure S4. The modification of SAMNs with TA did not influence the cyclic voltammograms with respect to bare SAMNs. Conversely, the modification of CPEs with 1% TA led to a reduction in the capacitive current at the electrodes and the appearance of a broad oxidation peak at +0.1 V, possibly due to the oxidation of the polyphenolic moieties of TA.

Commonly, material deposition on electrodes can be explored by using electrical impedance spectroscopy (EIS) in the presence of a redox couple, namely the ferricyanide/ferrocyanide redox system ($[Fe(CN)_6]^{3-/4-}$). Initially, cyclic voltammograms of CPEs modified with SAMNs and with SAMN@TA were recorded at a 50 mV s^{-1} scan rate in a 0.1 M PBS buffer solution that contained 5 mM $[Fe(CN)_6]^{3-/4-}$. As shown in Figure S5, all bare and modified electrodes exhibited reversible redox peaks, in which the bare CPE showed the highest peak-to-peak separation, $\Delta E = 239$ mV, and the lowest peak current density (see Table S4). The presence of TA led to two effects on the CPE response, that is, an increase in peak currents, which suggests improved electrocatalytic properties, and a decrease in the peak separation, which indicates an improved reversibility of the redox reactions. The interfacial properties of the modified electrodes were further evaluated by using EIS. The impedance between the electrode and the electrolyte solution can be

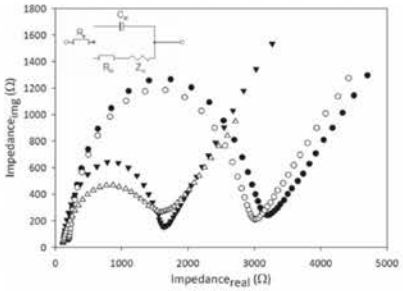

Figure 6. Characterization of modified CPEs by using electrical impedance spectroscopy. Nyquist plots of bare CPE (●) and CPEs modified with tannic acid (△), with SAMNs (○), and with SAMN@TA (▼). All measurements were performed in 0.1 mol L^{-1} PBS, pH 7.0, that contained $[Fe(CN)_6]^{3-/4-}$ redox probe (5 mmol L^{-1}) at an applied frequency range of 0.1 Hz to 100 kHz. An AC amplitude of 10 mV was applied. Inset: Randles equivalent circuit for the data fitting.

modeled simply by using the Randles equivalent circuit, as shown in Figure 6, inset. Impedance data are presented in Nyquist form in Figure 6, in which the semicircular part at higher frequencies corresponds to the electron-transfer-limited process and the linear part at lower frequencies corresponds to the diffusion process. The diameter of the semicircle is equal to the charge transfer resistance (R_{ct}), which controls the electron-transfer kinetics of the redox probe at the electrode interface. The large semicircle observed for the bare CPE indicates a high electron-transfer resistance. In the presence of TA/CPE, a smaller semicircle appeared and the R_{ct} value of SAMN@TA/CPE (1514.1 Ω) was almost two times lower than of bare CPE (2902.1 Ω), which indicates improved conductivity of the modified electrode (see Table S5). The same behavior was found for TA/CPE, which demonstrates successful immobilization of TA on the surface of the SAMNs. To test the electrocatalytic properties of SAMN@TA modified electrodes further, in comparison with the behavior of CPEs modified with bare SAMNs, different electroactive substances were used, that is, hydrogen peroxide, reduced nicotinamide adenine dinucleotide (NADH), and hydroquinone (HQ).

SAMNs demonstrated good electrocatalytic properties toward hydrogen peroxide reduction and were applied for the development of sensors.[52,53] For comparison, the electrocatalytic properties of the SAMN@TA complex were tested in the presence of H_2O_2 and Figure S4, inset, shows the cyclic voltammograms of CPEs modified with SAMN@TA in the presence of increasing concentrations of hydrogen peroxide.

Results of the chronoamperometry study are reported in Table S6. As shown, the response toward H_2O_2 was unaltered with respect to bare SAMNs, which confirmed the results obtained by using cyclic voltammetry (see Figure S4).

The sensitivity of SAMN@TA toward NADH was more than halved with respect to bare SAMNs, and showed a ten times higher limit of detection. In contrast, the response of SAMN@TA towards HQ was enhanced with respect to bare SAMNs. The corresponding typical current–time curve is shown in Figure S6. With respect to CPEs modified with bare SAMNs, the presence of SAMN@TA led to a 30% higher sensitivity and a four times lower detection limit. In this case, the calibration plot was linear ($I = 4.95 + 1.45$ [HQ]) in the 25 to 500 μM HQ concentration range. In 0.5 to 3 mM HQ, the electrode performance was characterized by slightly lower sensitivity (95.37 nA μM^{-1} cm^{-2}), even with good linearity (0.988). In this last case, the linear equation was $I = -9.019 + 1.362$ HQ. These results demonstrate that SAMN@TA/CPE can be proposed for the electrochemical determination of hydroquinone and derivatives.

The electrochemical behavior of SAMN@TA/CPE, compared with bare CPE, TA/CPE, and SAMN/CPE in the presence of the HQ/BQ (BQ = benzoquinone) redox couple was revealed by using cyclic voltammetry (see Figure S7 A). The introduction of the SAMN@TA complex in the CPE led to the lowest peak-to-peak potential difference with respect to the other modified and unmodified CPEs, which indicated the best electrochemical reversibility of the heterogeneous electron transfer reactions involving HQ oxidation and BQ reduction at the electrode surface (see Table S7). Furthermore, the influence of the potential scan rate on the registered CV peak currents in the presence of the HQ/BQ redox couple was also investigated (see Figure S7 B). The results revealed that the HQ oxidation peak depended linearly on the square root of the scan rate from 5 to 200 mV s^{-1}, which suggests that in this case the electron-transfer process is essentially diffusion-controlled (see Figure S7 C and Table S7).

Because the modification of CPEs by the introduction of the SAMN@TA complex led to specific electrocatalytic behavior for HQ oxidation, the possibility to detect HQ electrochemically was investigated by using square-wave voltammetry (SWV), as shown in Figure S8. The SAMN@TA-modified CPE, in the presence of 0.3 mM HQ, displayed a well-defined peak at +0.06 V with a peak area of (1340 ± 40) nC ($n = 3$), compared with (632 ± 41) nC ($n = 3$) calculated for the TA/CPE and (308 ± 22) nC for the SAMN/CPE ($n = 3$). The SWV oxidation peak of HQ at the SAMN@TA-modified CPE increased linearly with HQ concentration in the 25 to 500 μM range, and a calibration plot was constructed (see Figure 7). The sensitivity and the detection limit were 312.81 nC μM^{-1} cm^{-2} and 8.57 μM, respectively. The limit of detection was estimated as the signal-to-noise ratio (S/N 3).[54]

Because polyphenols in vegetal samples possess molecular structures derived from HQ (dihydroxybenzene derivatives and their polymers) and show the same redox behavior, we investigated the applicability of the proposed system for the determination of polyphenols in real samples, namely local blueberry extracts (see the Supporting Information). The amount of polyphenols in the samples was compared with the value obtained by using the Folin–Ciocalteu method,[55] which is considered a gold standard for polyphenol determination in plant extracts. The polyphenol content in blueberry samples determined by using the SAMN@TA electrodes was (89.9 ± 2.7)% ($n = 3$) with respect to the Folin–Ciocalteu method, which indicates that the proposed system can be successfully applied to real samples.

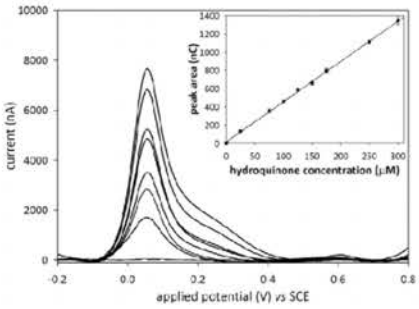

Figure 7. SWV response of SAMN@TA-modified CPE following the addition of HQ. Measurements were carried out in 0.1 mol L^{-1} PBS, pH 7.0; HQ final concentrations: 0, 25, 75, 100, 125, 150, 175, 250, 300 μmol L^{-1}. Inset: Calibration plot.

3. Conclusions

Herein, we reported on the development of stable and functional nanostructured ferric tannate interfaces on peculiar maghemite nanoparticles. The presence of surface under-coordinated iron(III) sites on nanoparticles acted, in the presence of TA in an aqueous solution, as nucleation seeds for the self-assembly of a ferric tannate nanoarchitecture (SAMN@TA). The nanomaterial was characterized by a considerably high stability constant according to a Langmuir isotherm study, so we envisage SAMNs as a potential tool for the magnetic removal of TA. The structure and electrochemical properties of the nanostructured SAMN@TA material were exhaustively characterized. Finally, the complex was applied for the development of a modified electrode aimed at the electrooxidation of polyphenols, which widened the application possibilities of both TA and maghemite nanoparticles due to a synergistic effect. The novel electrochemical properties of the SAMN@TA nanosensor were successfully used for to determine polyphenols in real samples, and thus represent a potential alternative to classical techniques.

Experimental Section

Chemicals were purchased at the highest commercially available purity and were used without further treatment. Iron(III) chloride hexahydrate (97%), sodium borohydride ($NaBH_4$), tannic acid (cat. 40304, 1701.23 g mol^{-1} molecular weight), and ammonia solution (35% in water) were obtained from Aldrich (Sigma–Aldrich, Italy). Methods are reported in the Supporting Information.

Acknowledgements

The present experimental work was partially funded by the Italian Institutional Ministry grants code 60A068055. The authors gratefully acknowledge the University of Padua (Italy), grant "Assegni di Ricerca Junior" 2014 n. CPDR148959 and the CARIPARO Foundation for support. The authors acknowledge support from the Ministry of Education, Youth and Sports of the Czech Republic (LO1305) and the Internal Student Grant of Palacky University in Olomouc, Czech Republic (project no. IGA_PrF_2015_017). The authors also acknowledge the assistance provided by the Research Infrastructure NanoEnviCz, supported by the Ministry of Education, Youth and Sports of the Czech Republic under project no. LM2015073.

Keywords: electrochemistry · iron oxide · nanoparticles · organic–inorganic hybrid composites · tannic acid

[1] P. G. Bruce, B. Scrosati, J. M. Tarascon, *Angew. Chem. Int. Ed.* **2008**, *47*, 2930–2946; *Angew. Chem.* **2008**, *120*, 2972–2989.
[2] J. Rocha, L. D. Carlos, F. A. A. Paz, D. Ananias, *Chem. Soc. Rev.* **2011**, *40*, 926–940.
[3] M. Sarikaya, C. Tamerler, A. K. Y. Jen, K. Schulten, F. Baneyx, *Nat. Mater.* **2003**, *2*, 577–585.
[4] E. Katz, I. Willner, *Angew. Chem. Int. Ed.* **2004**, *43*, 6042–6108; *Angew. Chem.* **2004**, *116*, 6166–6235.
[5] S. H. Jo, T. Chang, I. Ebong, B. B. Bhadviya, P. Mazumder, W. Lu, *Nano Lett.* **2010**, *10*, 1297–1301.
[6] G. H. Yu, L. B. Hu, M. Vosgueritchian, H. L. Wang, X. Xie, J. R. McDonough, X. Cui, Y. Cui, Z. N. Bao, *Nano Lett.* **2011**, *11*, 2905–2911.
[7] F. Hoffmann, M. Cornelius, J. Morell, M. Froba, *Angew. Chem. Int. Ed.* **2006**, *45*, 3216–3251; *Angew. Chem.* **2006**, *118*, 3290–3328.
[8] A. K. Cheetham, C. N. R. Rao, R. K. Feller, *Chem. Commun.* **2006**, *46*, 4780–4795.
[9] H. Goesmann, C. Feldmann, *Angew. Chem. Int. Ed.* **2010**, *49*, 1362–1395; *Angew. Chem.* **2010**, *122*, 1402–1437.
[10] J. F Liu, Z. S. Zhao, G. B. Jiang, *Environ. Sci. Technol.* **2008**, *42*, 6949–6954.
[11] N. A. Frey, S. Peng, K. Cheng, S. H. Sun, *Chem. Soc. Rev.* **2009**, *38*, 2532–2542.
[12] J. Hrbac, V. Halouzka, V. R. Zboril, K. Papadopoulos, T. Triantis, *Electroanalysis* **2007**, *19*, 1850–1854.
[13] H. Teymourian, A. Salimi, S. Khezrian, *Biosens. Bioelectron.* **2013**, *49*, 1–8.
[14] V. Urbanova, M. Magro, A. Gedanken, D. Baratella, F. Vianello, R. Zboril, *Chem. Mater.* **2014**, *26*, 6653–6673.
[15] M. Arruebo, R. Fernandez-Pacheco, M. R. Ibarra, J. Santamaria, *Nano Today* **2007**, *2*, 22–32.
[16] A. K. Gupta, M. Gupta, *Biomaterials* **2005**, *26*, 3995–4021.
[17] Q. A. Pankhurst, J. Connolly, S. K. Jones, J. Dobson, *J. Phys. D Appl. Phys.* **2003**, *36*, R167–R181.
[18] S. Altun, B. Çakıroğlu, M. Özacar, M. Özacar, *Colloids Surf. B* **2015**, *136*, 963–970.
[19] M. Bagtash, Y. Yamini, E. Tahmasebi, J. Zolgharnein, Z. Dalirnasab, *Microchim. Acta* **2016**, *183*, 449–456.
[20] J. H. Wang, C.-L. Zheng, S. L. Ding, H. R. Ma, Y. F. Ji, *Desalination* **2011**, *273*, 285–291.
[21] K. Atacan, M. Özacar, *Colloids Surf. B* **2015**, *128*, 227–236.
[22] C. Nadejde, M. Neamtu, V.-D. Hodoroaba, R. J. Schneider, A. Paul, G. Ababei, U. Panne, *J. Nanopart. Res.* **2015**, *17*, 476.
[23] M. Magro, G. Sinigaglia, L. Nodari, J. Tucek, K. Polakova, Z. Marusak, S. Cardillo, G. Salviulo, U. Russo, R. Stevanato, R. Zboril, F. Vianello, *Acta Biomater.* **2012**, *8*, 2068–2076.
[24] M. Magro, L. Nodari, U. Russo, G. Valle, F. Vianello, US Patent 8, 980, 218 **2015** March 17.
[25] M. Magro, A. Faralli, D. Baratella, I. Bertipaglia, S. Giannetti, G. Salviulo, R. Zboril, F. Vianello, *Langmuir* **2012**, *28*, 15392–15401.
[26] G. Sinigaglia, M. Magro, G. Miotto, S. Cardillo, E. Agostinelli, R. Zboril, E. Bidollari, F. Vianello, *Int. J. Nanomedicine* **2012**, *7*, 2249–2259.
[27] G. Miotto, M. Magro, M. Terzo, M. Zaccarin, L. Da Dalt, E. Bonaiuto, D. Baratella, G. Gabai, F. Vianello, *Colloids Surf. B* **2016**, *140*, 40–49.
[28] K.-T. Chung, T. Y. C. Wong, C. I. Wei, Y. W. Huang, Y. Lin, *Crit. Rev. Food Sci. Nutr.* **1998**, *38*, 421–464.
[29] A. Roche, E. Ross, N. Walsh, K. O'Donnell, A. Williams, M. Klapp, N. Fullard, S. Edelstein, *Crit. Rev. Food Sci. Nutr.* **2015**, DOI: 10.1080/10408398.2013.865589.
[30] M. Favre, D. Landolt, *Corros. Sci.* **1993**, *34*, 1481–1494.

[31] M. Favre, D. Landolt, K. Hoffman, M. Stratmann, *Corros. Sci.* **1998**, *40*,793 – 803.
[32] J. Gust, *Corrosion-NACE* **1991**, *47*, 453 – 457.
[33] D. Landolt, M. Favre in *Progress in the Understanding and Prevention of Corrosion* (Eds.: J. M. Costa, A. D. Mercer), Institute of Materials, London, UK **1993**, pp. 374 – 386.
[34] S. Nasrazadani, *Corros. Sci.* **1997**, *39*, 1845 – 1859.
[35] J. Gust, J. Suwalski, *Corrosion-NACE* **1994**, *50*, 355 – 365.
[36] Iglesias, E. G. De Saldaña, J. A. Jaen, *Hyperfine Interact.* **2001**, *134*, 109 – 114.
[37] L. C. Katwa, M. Ramakrishna, M. R. R. Rao, *J. Biosci.* **1981**, *3*, 135 – 142.
[38] S. Yahya, A. M. Shah, A. A. Rahim, N. H. A. Aziz, R. Roslan, *J. Phys. Sci.* **2008**, *19*, 31 – 41.
[39] M. Magro, D. Baratella, P. Jakubec, G. Zoppellaro, J. Tucek, C. Aparicio, R. Venerando, G. Sartori, F. Francescato, F. Mion, N. Gabellini, R. Zboril, F. Vianello, *Adv. Funct. Mater.* **2015**, *25*, 1822 – 1831.
[40] I. Langmuir, *J. Am. Chem. Soc.* **1918**, *40*, 1361 – 1403.
[41] J. Y. Yang, C. P. Swaminathan, Y. Huang, R. J. Guan, S. W. Cho, M. Kieke, D. M. Kranz, R. A. Mariuzza, E. J. Sundberg, *J. Biol. Chem.* **2003**, *278*, 50412 – 50421.
[42] H. G. Hong, W. A. Park, *Electrochim. Acta* **2005**, *51*, 579 – 587.
[43] M. L. Pisarchick, N. L.; Thompson, *Biophys. J.* **1990**, *58*, 1235 – 1249; Thompson, *Biophys. J.* **1990**, *58*, 1235 – 1249.
[44] Y. H. Deng, L. Wang, X. B. Hu, B. Z. Liu, Z. B. Wei, S. G. Yang, C. Sun, *Chem. Eng. J.* **2012**, *181*, 300 – 306.
[45] L. C. Fu, F. Q. Liu, Y. Ma, X. W. Tao, C. Ling, A. M. Li, C. D. Shuang, Y. Li, *Chem. Eng. J.* **2015**, *263*, 83 – 91.
[46] R. Kumar, M. A. Barakat, E. M. Soliman, *J. Ind. Eng. Chem.* **2014**, *20*, 2992 – 2997.
[47] J. W. Lin, Y. H. Zhan, Z. L. Zhu, Y. Q. Xing, *J. Hazard. Mater.* **2011**, *193*, 102 – 111.
[48] M. Magro, R. Campos, D. Baratella, G. Lima, K. Hola, C. Divoky, R. Stollberger, O. Malina, C. Aparicio, G. Zoppellaro, R. Zboril, F. Vianello, *Chem. Eur. J.* **2014**, *20*, 11913 – 11920.
[49] M. Magro, D. E. Moritz, E. Bonaiuto, D. Baratella, M. Terzo, P. Jakubec, O. Malina, K. Čépe, G. M. F. de Aragao, R. Zboril, F. Vianello, *Food Chem.* **2016**, *203*, 505 – 512.
[50] T. Rajh, L. X. Chen, K. Lukas, T. Liu, M. C. Thurnauer, D. M. Tiede, *J. Phys. Chem. B* **2002**, *106*, 10543 – 10552.
[51] J. A. Jaen, J. De Obaldia, M. V. Rodriguez, *Hyperfine Interact.* **2011**, *202*, 25 – 38.
[52] D. Baratella, M. Magro, G. Sinigaglia, R. Zboril, G. Salviulo, F. Vianello, *Biosens. Bioelectron.* **2013**, *45*, 13 – 18.
[53] M. Magro, D. Baratella, N. Pianca, A. Toninello, S. Grancara, R. Zboril, F. Vianello, *Sens. Actuators. B Chem.* **2013**, *176*, 315 – 322.
[54] E. Desimoni, B. Brunetti in *Environmental Analysis by Electrochemical Sensors and Biosensors—Applications*, Vol. 2, 1st ed. (Eds.: L. M. Moretto, K. Kalcher), Springer, New York, **2015**, pp. 1137 – 1151.
[55] K. W. Lee, Y. J. Kim, H. J. Lee, C. Y. Lee, *J. Agric. Food Chem.* **2003**, *51*, 7292 – 7295.

Manuscript received: July 3, 2016
Accepted Article published: July 28, 2016
Final Article published: August 19, 2016

7.3- Innovative core-shell nanocarrier, SAMN@TA, applied to test the antimicrobial properties of SAMN@TA on *Listeria monocytogenes.*

Publication number 3:

de Almeida Roger, J. Magro, M. Spagnolo, S. Bonaiuto, E. Baratella, D. Fasolato, L. Vianello, L. Massimiliano. Antimicrobial and magnetically removable tannic acid nanocarrier: A processing aid for *Listeria monocytogenes* treatment for food industry applications. 2017. Food chemistry. https://doi.org/10.1016/j.foodchem.2017.06.109.

ARTICLE IN PRESS

Food Chemistry xxx (2017) xxx–xxx

Contents lists available at ScienceDirect

Food Chemistry

journal homepage: www.elsevier.com/locate/foodchem

Antimicrobial and magnetically removable tannic acid nanocarrier: A processing aid for *Listeria monocytogenes* treatment for food industry applications

Jessica de Almeida Roger [a], Massimiliano Magro [a,b], Silvia Spagnolo [a], Emanuela Bonaiuto [a], Davide Baratella [a], Luca Fasolato [a,*], Fabio Vianello [a,b,*]

[a] Department of Comparative Biomedicine and Food Science, University of Padua, Italy
[b] Regional Centre of Advanced Technologies and Materials, Department of Physical Chemistry and Experimental Physics, Palacky University, Olomouc, Czech Republic

ARTICLE INFO

Article history:
Received 1 March 2017
Received in revised form 14 June 2017
Accepted 20 June 2017
Available online xxxx

Chemical compounds studied in this article:
Tannic acid (PubChem CID: 16129778)

Keywords:
Tannic acid
Magnetic nanoparticles
Listeria monocytogenes
Bacteria removal
Bacteriostatic
Nanohybrid

ABSTRACT

An innovative core-shell nanocarrier, combining the magnetism of surface active maghemite nanoparticles (SAMNs, the core) and tannic acid (TA, the shell) was self-assembled by simple incubation in water. Due to the drastic reorganization of SAMN surface, the prepared magnetic nanocarrier (SAMN@TA) resulted as one of the most robust nanomaterial bearing TA to date. Nevertheless, the ferric tannates network, constituting the SAMN@TA shell, and the free tannic acid display comparable chemical behavior. The antimicrobial properties of SAMN@TA were tested on *Listeria monocytogenes* in comparison with free TA, showing similar bacteriostatic effects at relatively low concentrations. Besides the preservation of the TA inhibitory activity toward *L. monocytogenes*, the possibility of being magnetically removed leaving no residues into the matrix makes this nanocarrier an innovative processing aid for surface treatments. Thus, SAMN@TA can be used as an effective, low-cost and environmentally friendly antimicrobial nanomaterial for the food industry applications.

1. Introduction

The control of foodborne pathogens represents a crucial task as a mean to reduce significantly the possibility of disease outbreaks (Kiran-kumar, Badarinath, & Halami, 2008). In an attempt to prevent this problem, food industries normally use synthetic preservatives and antibiotics in the food production processes for eliminating microorganisms. However, the combination of excessive and inappropriate use of chemical substances led to the emergence of drug resistance in bacteria, increasing the difficulty of controlling the proliferation of foodborne diseases.

The interest in natural alternatives to antibiotics and classical preservatives is rapidly increasing for reducing chemicals and avoiding bacterial resistance, and may represent a new strategy against microbial infections (David, Steenson, & Davidson, 2013). Among natural substances, phenolic compounds have been shown to exert antioxidant, anti-inflammatory, anti-cancer and antibacterial activity. Indeed, phenolic compounds are a class of biomolecules known for their antimicrobial action (Coppo & Marchese, 2014; Gyawali & Ibrahim, 2014; Kim, Kang, & Kim, 2011; Lagha, Dudonné, Desjardins, & Grenier, 2015), and were proposed as natural food preservatives against foodborne bacteria (Coppo & Marchese, 2014).

Phenolic compounds are widely distributed in natural products, such as fruits, vegetables and seeds, and constitute one of the largest and most ubiquitous class of secondary metabolites in the plant kingdom. They comprise, as common motif, molecular structures with at least one aromatic ring, substituted with one or more hydroxyl moieties (Fig. 1, panel A). Most phenols of natural origin have at least two hydroxyls in their structure and are characterized by a wide structural diversity.

* Corresponding authors at: Department of Comparative Biomedicine and Food Safety, University of Padua, Agripolis – Viale dell'Università 16, Legnaro 35020 (PD), Italy.
E-mail addresses: jessicabiotecnologia@gmail.com (J. de Almeida Roger), massimiliano.magro@unipd.it (M. Magro), silvia.spagnolo89@gmail.com (S. Spagnolo), emanuela.bonaiuto@unipd.it (E. Bonaiuto), davide.baratella.1@studenti.unipd.it (D. Baratella), luca.fasolato@unipd.it (L. Fasolato), fabio.vianello@unipd.it (F. Vianello).

http://dx.doi.org/10.1016/j.foodchem.2017.06.109
0308-8146/

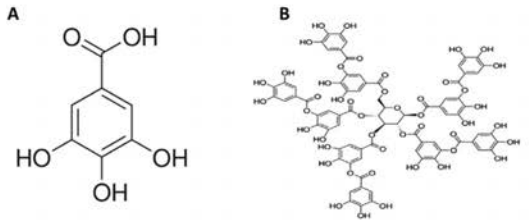

Fig. 1. Structure of a simple phenolic compound and of tannic acid. A) Molecular structure of gallic acid B) Molecular structure of tannic acid.

Among phenolic compounds, tannic acid (TA), is a widely spread polyphenol, characterized by an effective inhibition of bacterial growth, see panel B of Fig. 1 (Coppo & Marchese, 2014). Molecularly, TA (IUPAC name: 2,3-dihydroxy-5-({[(2R,3R,4S,5R,6R)-3,4,5,6-tetrakis({3,4-dihydroxy-5-[(3,4,5-trihydroxyphenyl)-carbonyloxy]-phenyl}carbonyloxy)oxan-2-yl]methoxy}carbonyl) phenyl-3,4,5-trihydroxybenzoate) affects several metabolic pathways in bacteria cells, where it can reduce iron intake, due to its chelating properties toward transition metals, leading to a modulation of cellular oxidative stress (Lim, Penesyan, Hassan, Loper, & Paulsen, 2013). Bacterial swimming motility and biofilm formation are also affected by TA, possibly due to iron ions depletion or to the direct binding of TA to cell surface structures, such as lipo-polysaccarides and flagellin (Lim et al., 2013; O'May & Tufenkji, 2011). These effects are of greater concerns for the food industry, where biofilm formation is a matter of concern, especially for foodborne pathogen, such as *Listeria monocytogenes*.

L. monocytogenes can cause listeriosis, which is a severe disease with high hospitalization and a case-fatality rate up to 30% (Buchanan, Gorris, Hayman, Jackson, and Whiting, 2017; Lomonaco, Nucera, & Filipello, 2015; Mead et al., 1999; Muñoz et al., 2012). Both outbreaks and sporadic cases are associated with contamination of various types of food, such as milk, soft cheese, meat, vegetables and seafood products. The ubiquitous nature of this foodborne pathogen and its growth ability at low temperatures concur to its survival and maintenance in the food industry plants. Indeed *L. monocytogenes* can persist for long time in the form of biofilm on the surfaces of the processing plant, and even in the refrigerated food final products (Simões, Simões, & Vieira, 2010).

The use of natural compounds could be a new eco-friendly system to control *L. monocyto*genes contamination of food and biofilm formation. The strong activity of tannin rich fraction of pomegranate against *L. monocytogenes* cell membrane, was documented (Li et al., 2014). Accordingly, Cetin-Karaca and Newman (2015) described the antimicrobial activity of TA on *L. monocytogenes*, showing a minimal inhibitory concentration (MIC) below 20 μg/mL, after 60 h of incubation. Concerning its real applicability in food industry, tannic acid can not be considered a processing aid as it can be hardly removed from food matrixes once added.

In the last years, nanotechnology emerged as sophisticated platform for responding to the need of novel strategies at molecular level (Bohara & Pawar, 2015), and represents a new frontier in food industry, finding potential applications in every segment of the production process. Nanomaterials can be employed as supports for the immobilization of substances of interest enhancing their bioavailability, creating magnetically drivable vehicles (Magro, Campos et al., 2014) and providing targeting functionalities, which can improve delivered drug efficacy. Furthermore, nanomaterials can provide competitive methods for the identification, capture and inhibition of bacteria (Inbaraj & Chen, 2015).

Recently, we developed a new type of magnetic nanoparticles, consisting of a nanostructured superparamagnetic iron oxide constituted of stoichiometric maghemite (γ-Fe_2O_3), with a size around 10 nm, and presenting peculiar surface chemical behavior (Magro, Sinigaglia et al., 2012). These nanoparticles were named "surface active maghemite nanoparticles" (SAMNs). SAMNs show excellent water stability, as colloidal suspensions, without any organic or inorganic surface coating, and a high average magnetic moment, allowing an easy magnetic driving. Due to SAMN peculiar properties, they were already used for immobilizing different biomolecules (Magro, Faralli et al., 2012; Magro, Baratella et al., 2015) and proposed for the development of biosensors (Baratella et al., 2013; Bonaiuto et al., 2016; Magro et al., 2013), and for biomedical applications (Cmiel et al., 2016; Skopalik et al., 2014; Venerando et al., 2013), biotechnology (Magro, Faralli et al., 2012) and food industry (Magro, Baratella et al., 2014; Magro, Esteves et al., 2016; Miotto et al., 2016). In particular, we prepared and characterized a novel hybrid nanomaterial by coating SAMNs with TA (SAMN@TA). SAMN@TA complex resulted extremely stable and was structurally and electrochemically characterized and successfully applied for the development of an electrochemical sensor (Magro, Fasolato et al., 2016). In the present report, the antimicrobial properties of the nanostructured SAMN@TA hybrid complex were tested against *Listeria monocytogenes*, and proposed as processing aid for surface treatment, without leaving residues in the matrix.

2. Material and methods

Chemicals were purchased at the highest commercially available purity and were used without further treatment. Iron(III) chloride hexahydrate (97%), sodium borohydride (NaBH4), tannic acid ((IUPAC name: 2,3-dihydroxy-5-({[(2R,3R,4S,5R,6R)-3,4,5,6-tetrakis({3,4-dihydroxy-5-[(3,4,5-trihydroxyphenyl)-carbonyloxy]-phenyl}carbonyloxy)oxan-2-yl]methoxy}carbonyl)phenyl-3,4,5-trihydroxybenzoate, cat. 40304, 1701.23 $gmol^{-1}$ molecular weight), and ammonia solution (35% in water) were obtained from Aldrich (Sigma–Aldrich, Italy).

2.1. Synthesis of nanoparticles

A typical nanoparticles were synthesized as previously described (Magro, Valle, Russo, Nodari, & Vianello, 2012) and can be summarized as follows: $FeCl_3{\cdot}6H_2O$ (10.0 g, 37 mmol) was dissolved in Milli-Q grade water (800 mL) under vigorous stirring at room temperature. $NaBH_4$ solution (2.0 g, 53 mmol) in ammonia (3.5%, 100 mL, 4.86 mol/mol Fe) was then quickly added to the mixture. After the reduction reaction occurrence, the temperature was increased up to 100 °C and kept constant for 2 h, under stirring. Then, the system was cooled at room temperature and aged in water for 12 h. The magnetic product was separated by imposition of an external magnet for 60 min, and washed three times with water. The resulting material can be transformed into a red brown powder (final synthesis product) by curing at 400 °C for 2 h, leading to individual nanoparticles. The resulting nanopowder showed a high magnetic response upon exposure to a magnetic field. The final Fe_2O_3 mass was 2.0 g (12.5 mmol) and a yield of 68% was calculated. The obtained naked iron oxide nanomaterial leads to a stable colloidal suspension in water upon sonication (Bransonic, model 221, 48 kHz, 50 W).

2.2. Magnetic separation

A series of Nd–Fe–B magnets (N35, 263-287 kJ/m^3 BH, 1170-1210 mT flux density by Powermagnet, Germany) were used for

Please cite this article in press as: de Almeida Roger, J., et al. Antimicrobial and magnetically removable tannic acid nanocarrier: A processing aid for *Listeria monocytogenes* treatment for food industry applications. *Food Chemistry* (2017), http://dx.doi.org/10.1016/j.foodchem.2017.06.109

the magnetic separations. Magnets were applied on the bottom of the reaction flasks, and depending on the flask volume, supernatants were separated by suction after 30–60 min.

2.3. Derivatization of SAMNs with tannic acid

The core-shell hybrid nanomaterial (SAMN@TA) constituted of SAMNs (the core) and tannic acid (TA, the shell) was prepared as follows (Magro, Fasolato et al., 2016): a colloidal dispersion of naked SAMNs (400 mg L^{-1}) was prepared in house and subsequently derivatized with TA (200 mg L^{-1}) by simple incubation in water overnight at 25 °C. After the incubation period, the nanoparticles were separated by application of an external magnet and extensively washed with water. The amount of TA bound on SAMNs was calculated from the disappearance of the absorbance at 280 nm in the supernatants ($\varepsilon_{280nm} = 6.99 \times 10^4\ M^{-1}\ cm^{-1}$). The final amount of TA on nanoparticle surface was 200 mg/g SAMN. Once prepared the SAMN@TA complex was suspended in Phosphate-Buffered Saline (PBS) for further experiments.

2.4. Quantitative assay for the minimum inhibitory concentration

A standardized inoculum of *L. monocytogenes* (ATCC 19117) was used for experiments. The strains were plated on ALOA (Biolife Italiana srl, Milano, Italy) and incubated at 37 °C for 19 h. Pure colonies were suspended in 10 mL Mueller Hinton Broth (MHB, Biolife Italiana srl, Milano, Italy) and diluted until the concentration was 5.0 Log_{10} CFU (colony forming unit)/ml.

The microbroth dilution technique of antimicrobial susceptibility was performed to test the inhibitory effect on the growth of *Listeria monocytogenes*. Serial two fold dilutions of the SAMN@TA complex (25, 50, 100 and 200 mg L^{-1}) were carried out in 96-well flat bottom micro-titer plates (Sarstedt, Nümbrecht, Germany) and incubated with standardized inoculum (100 μL). Control experiments on *L. monocytogenes* were carried out in the presence of free TA (6.75, 12.5, 25 and 50 mg L^{-1}).

The microtiter assays were incubated at 37 °C and the optical density (OD_{600}) was continuously monitored by spectrophotometry for 24 h using a Spectrophotometer Multiskan GO Microplate Readers (Thermo Fisher Scientific, Waltham, Massachusetts, USA). In order to correct the possible absorbance interferences due to the oxidation of free and bound TA, control experiments were performed (Tsai, Tsai, Chien, Lee, & Tsai, 2008).

The minimum inhibitory concentration (MIC) was defined as the lowest concentration of the substance that inhibited the bacterial growth in comparison with the control. As a threshold, the concentration that limited the increase of turbidity to < 0.05 absorbance was adopted (Tsai et al., 2008). After 24 h incubation, the minimum lethal concentration (MLC) was also performed by striking 10 μL broth cultures on TSAYE medium (Tryptone Soy Agar supplemented with 0.6% yeast extract (YE) by Oxoid) at 37 °C for 48 h. MLC was defined as the lowest concentration leading to no visible growth. Three different biological replicates were performed for each plate and all experiments were performed in triplicate.

2.5. Determination of capture efficiency (CE)

Capture efficiency (CE) was estimated as the percentage of cells that interact with nanoparticles (100 mg L^{-1}) and were consequently removed from the liquid medium using an external magnet. Standardized pre-inoculums were prepared according to the above mentioned method, and experiments were conducted with the initial populations of 3.0 log_{10} CFU/ml. Each experiment was performed in sterile test tubes at a 2 mL final volume incubated at room temperature (22 °C) for 30 min with or without gently mixing. After the incubation period, a magnetic separation was performed (30 min) and the supernatants were removed. As defined by preliminary experiments, the pellets were washed and re-suspended in fresh PBS. No effects of wall retention or adsorption on the test tubes were observed. Finally, the number of microbial cells were estimated in the supernatants and re-suspended pellets. Serial 10-fold dilutions were performed in PBS medium and then 100 μL of each dilution was inoculated by spread-plate method on TSBYE plates. The results were reported as log_{10} CFU (colony forming units)/mL. The capture efficiency (CE) was calculated according to the equation reported by Xiong et al. (2014):

$$CE\ (\%) = \left(1 - \frac{C_b}{C_0}\right) \times 100$$

where C_0 represented the total CFU in the samples and C_b the CFU in the supernatant.

3. Results and discussion

3.1. Characterization of the complex between magnetic nanoparticles (SAMNs) and tannic acid (TA): The SAMN@TA nanocarrier

The nanoparticulated SAMN@TA hybrid was synthetized according to the method described by Magro, Fasolato et al. (2016), and an HR-TEM micrograph of the as prepared SAMN@TA complex is reported in Fig. 2, where a coating characterized by a lower electrondensity compatible with the expected ferric tannate shell of approximately 2.0 nm thickness on the magnetic core is evident. The nature of the core of the witnessed self-assembly core-shell nanostructure is easily attributable to maghemite nanoparticles, as shown in Fig. 2, inset. In fact, the value of measured interplanar distances resulted to be 2.9 Å, which perfectly matches with the γ-Fe_2O_3 crystal (220) Miller index (Guivar et al., 2014).

As the aim of the present work was to study the effects of the SAMN@TA complex on *L. monocytogenes* cells, it was important to prepare and characterize stable colloidal suspensions of the hybrid nanomaterial (Yu & Xie, 2012). Thus, the resuspension kinetics of SAMN@TA (0.10 g) in bi-distilled water (500 mL) was examined using an ultrasonic bath (Falc Instruments, Italy, mod. LBS1, 50–60 Hz, 500 W). Starting from the dried nanomaterial,

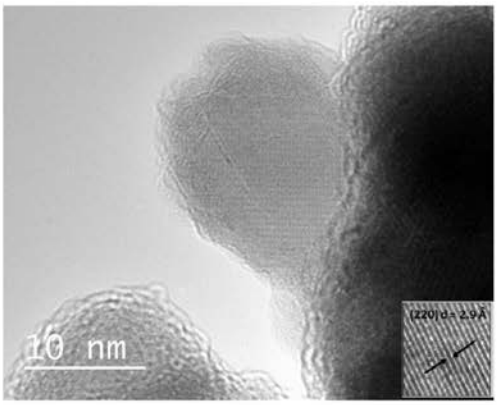

Fig. 2. TEM image of the SAMN@TA complex. Inset: high-magnification of SAMN@TA complex by HR-TEM evidencing crystal planes and the characteristic interplanar distances of the well-conserved γ-Fe_2O_3 lattice.

Please cite this article in press as: de Almeida Roger, J., et al. Antimicrobial and magnetically removable tannic acid nanocarrier: A processing aid for *Listeria monocytogenes* treatment for food industry applications. *Food Chemistry* (2017). http://dx.doi.org/10.1016/j.foodchem.2017.06.109

the formation of the colloidal suspension was followed by monitoring the optical absorption spectrum at 420 nm (Magro, Fasolato et al., 2016). As reported in our earlier study (Magro, Sinigaglia et al., 2012), the interaction of an organic molecule (tannic acid) with SAMN surface leads to a modification of the nanoparticle optical properties. In particular, the wide absorption band of SAMN@TA is characterized by a maximum absorption at 420 nm and a shoulder at 490 nm and followed along with the ultrasound application process. The increase of suspension absorbance at 420 nm during sonication exhibited exponential behavior, characterized by a kinetic constant of 0.85 h^{-1}, which was superimposable to the resuspension behavior of naked SAMNs (Sinigaglia et al., 2012).

During the resuspension process in water, pH values decreased from 5.5 to 4.0, as the reddish brown nanoparticulated powder was subjected to ultrasound treatment, indicating that the reorganization of SAMN surface into ferric tannates leads to the development of an acidic interface.

At the accomplishment of the ultrasound induced resuspension, the obtained stable colloidal suspension of SAMN@TA (200 mg L^{-1}) was titrated using a pH-meter (basic 20, Crison). The resulting titration curve indicated a pKa at pH 10.5, attributable to the phenolic hydrogens of TA molecule (Costadinnova, Hristova, Kolusheva, & Stoilova, 2012) and an additional pKa at around pH = 6.0, (Fig. 3). According to Fazary, Taha, and Ju (2009), the chelation of iron(III) by polyphenols induces a drastic shift of the pKa of phenolic hydroxyls to lower pH values. Thus, this lower pKa can be attributable to the involvement of the polyphenol in the metal surface complexation of SAMNs, which lead to the formation of the ferric tannate network of SAMN@TA. The availability of these hydroxyl groups (-OH) can explain the observed nanohybrid acidity. Taking into account that the number of phenolic -OH per single TA molecule is 25, and that the amount of polyphenols on the metal oxide surface corresponds to about 1.2 TA molecules per nm^2 (Magro, Fasolato et al., 2016), it is possible to calculate the surface density of phenolic -OH on SAMN@TA, which corresponds to 37.5 OH groups per square nanometer. On the basis of previously determined surface area of maghemite nanoparticles by BET (46.23 $m^2 g^{-1}$) (Magro, Baratella et al., 2014), the surface density of -OH obtained from the experimental titration curve is in agreement with this value (39 -OH per square nanometer). This suggests that the availability of -OH on the ferric tannate layer shelling the SAMN@TA nanocarrier are comparable to those of the free TA. Therefore, such a similarity could explain the similar behavior with respect to the growth inhibition of *L. monocytogenes* (see hereafter).

3.2. Magnetic separation of L. Monocytogenes by SAMN@TA

Macromolecules on the bacterial cell surface, such as flagellin and lipo-polysaccarides, were proposed as possible targets involved in the interaction with tannic acid (Lim et al., 2013; O'May et al., 2011). Recently, informative insights on nanoparticle-bacteria interactions were provided by SAMNs as magnetically drivable probe in the study of iron uptake regulation and mineral adhesion mechanism in *Pseudomonas fluorescens* (Magro, Bonaiuto et al., 2016). Thus, in order to test the interactions between *L. monocytogenes* and SAMN@TA, capture studies were performed via simple magnetic separation.

Capture efficiency (CE) of SAMN@TA on *L. monocytogenes* was estimated as the percentage of bacterial cells that interacted with nanoparticles (100 mg L^{-1}) and were consequently removed from the liquid medium using an external magnet, as described in Methods.

Noteworthy, as shown in Table 1, CE was relevant both in the presence and in absence of agitation, indicating the occurrence of a strong interaction between SAMN@TA and bacterial cells. Agitation led to a 50% higher CE, probably by favouring a higher number of effective collisions between the nanomaterial and microorganisms.

Interestingly, after the magnetic separation, the number of microbial cells in the pellets revealed a different behavior. Conversely to the pellet obtained from the cultures subjected to agitation, in which about 90.0% of captured cell grew regularly, in the absence of agitation the growth of microorganisms was drastically inhibited. According to the plate count (see Materials and Methods), only 2.0% of the magnetically recovered cells resulted to grow on plate, suggesting the occurrence of aggregation phenomena. Similarly to growth inhibition, the capture efficiency depended on the concentration of SAMN@TA (see next paragraph). Actually, the two phenomena were a function of the fraction of bacteria population interacting with SAMN@TA. As reported below, at 200 mg L^{-1} SAMN@TA, the bacterial growth was completely zeroed, showing that SAMN@TA can interact with the whole bacterial

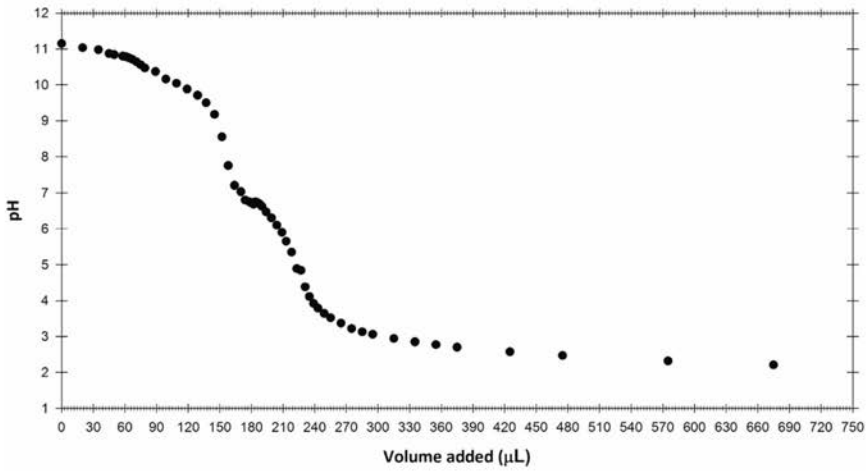

Fig. 3. Titration curve of the SAMN@TA complex.

Please cite this article in press as: de Almeida Roger, J., et al. Antimicrobial and magnetically removable tannic acid nanocarrier: A processing aid for *Listeria monocytogenes* treatment for food industry applications. *Food Chemistry* (2017), http://dx.doi.org/10.1016/j.foodchem.2017.06.109

Table 1
Capture efficiency of SAMN@TA on *L. monocytogenes*.

Incubation	Bacteria concentration LogCFU/mL	Capture efficiency (%)*
Static	4.52 ± 0.58	43.49 ± 4.60
Agitation	4.14 ± 0.08	66.25 ± 4.48

* Capture efficiency supernatant (%) = (1–(number of cells from supernatant/total cell number of initial samples)) × 100.

population. Under these conditions, the removal of bacterial cells was easily accomplished. On the other hand, as in the case of bacteria capture under static conditions, the successful capture cannot be adequately demonstrated by plate count, probably because of excessive aggregation. It should be considered that surveys on raw milk, as an example of contaminated liquid food products, showed that the concentration of *L. monocytogenes* in positive samples was usually less than 1 $\log_{10}$ (King, Lake, & Cressey, 2014; Waak, Tham, & Danielsson-Tham, 2002). Our results suggest that the SAMN@TA complex was able to remove about 4 Log_{10}, which is the level often releaved in the case of elevate contamination (e.g. mastitic milk) (King et al., 2014). Notably, the treatment of highly contaminated products is feasible increasing SAMN@TA concentration. Therefore, besides demonstrating the proclivity of interacting with *L. monocytogenes*, SAMN@TA can be proposed as a tool for the magnetic removal of this bacterium, as well as for its determination in plate.

3.3. Minimum inhibitory concentration (MIC) of SAMN@TA on L. Monocytogenes

The determination of MIC, and of other endpoint assays, is a crucial step for the characterization of a novel antimicrobial agent for the food industry. Moreover, liquid assays provide an accurate evaluation of growth inhibition also in dynamic studies, where the decrease of absorbance and the delay of bacterial lag phases are considered as a success criterion for future applications (David et al., 2013).

The effect of the SAMN@TA nanocarrier on the growth of *L. monocytogenes* was studied and compared to free tannic acid (TA) in the concentration range comprised between 6.75 and 100 mg L^{-1} (see Fig. 4).

The MIC values were assessed according to the threshold proposed by Tsai et al. (2008), and, as a conservative interpretation, the MIC concentrations were considered when all experimental replicates show an increase of absorbance <0.05 OD_{600}. After 24 h incubation, MIC values of free TA resulted of 25 mg L^{-1}, in good agreement with other studies performed by applying free TA and TA in nanocomposites. Literature reported similar values for TA against gram-negative such as *Pseudomonas aeruginosa*, *Salmonella* and *Escherichia coli* and gram positive bacteria, such as *Staphylococcus aureus* and *L. monocytogenes* (Cetin-Karaca 2011; Kim, Cha, Cho, & Park, 2016).

The MIC value showed by SAMN@TA on *L. monocytogenes* was at 100 mg L^{-1}. Considering that TA represents 20.0% w/w of the SAMN@TA complex, MIC values resulted similar for SAMN@TA and free TA. This further proves the comparable surface chemistry of the ferric tannate layer shelling the SAMN@TA complex and the free TA, probably due to the conserved availability of phenolic hydroxyls upon interaction with maghemite. In fact, in contrast with the drastic reorganization of SAMN surface upon TA binding, the final nanostructured ferric tannates maintains the inhibitory activity of free TA on *L. monocytogenes*. Moreover, the growth behavior of *L. monocytogenes* resulted influenced by the presence of SAMN@TA, showing longer lag times and a reduction of the OD values. The bacterial growth was completely zeroed at 200 mg L^{-1} SAMN@TA.

The interaction of SAMN@TA with bacteria led to the formation of aggregates, which tend to precipitate in PBS. Pellets were studied in order to verify if the process affects the vitality of bacterial cells. Thus, after 24 h of incubation in the presence of SAMN@TA and TA, bacterial suspensions and pellets were plated on TSAYE medium in order to evaluate the minimum lethal concentration (MLC). Interestingly, *L. monocytogenes* formed visible colonies at all the studied concentrations (6.75, 12.5, 25 and 50 μg/mL), suggesting that SAMN@TA, as free TA, shows a bacteriostatic effect and not the bactericidal activity.

Magnetic capture ability and inhibitory activity of SAMN@TA could be advantageously used for cleaning purposes and to reduce the potential growth of *L. monocytogenes* during food processing. Moreover, thanks to the magnetic properties of the maghemite nanoparticles, the SAMN@TA complex can be applied as processing aid, which can be eventually removed from the final product. It should be stressed that the magnetic properties correlated with the maghemite core of SAMN@TA offer the advantage of performing the removal of *L. monocytogenes* from the matrix by the application of external magnetic field, allowing a subsequent bacteria quantification by microbiological assays.

The described laboratory approach has shown potential to be used as antimicrobial agent for the food industrial applications. Indeed, a recent publication reported on a patented prototype plant (Bettinsoli et al., 2016), consisting of a simple modular robotic platform, which was successfully applied for environmental remediation (Magro, Domeneghetti et al., 2016). The proposed robotic system can be easily applied on liquid food products for the magnetic removal of *L. monocytogenes*. Note that all these operations are possible because of the peculiar colloidal stability of SAMN@TA, their surface reactivity, and the fast binding kinetics. In addition, the synthetic protocol for SAMNs and the TA coating

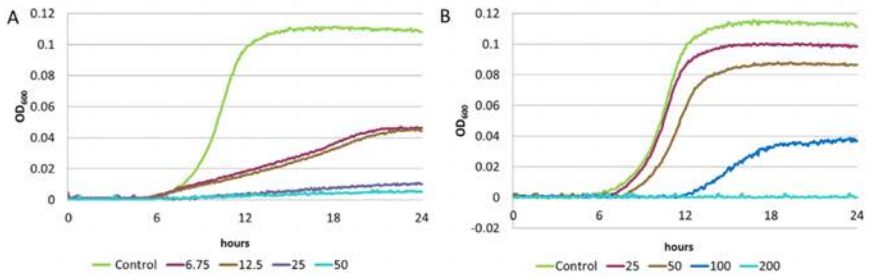

Fig. 4. Growth curves of *L. monocytogenes* in the presence of free tannic acid (A) and SAMN@TA (B). Data are reported as the average of the 3 experimental replicates. The concentrations were expressed as mg L^{-1}.

Please cite this article in press as: de Almeida Roger, J., et al. Antimicrobial and magnetically removable tannic acid nanocarrier: A processing aid for *Listeria monocytogenes* treatment for food industry applications. *Food Chemistry* (2017). http://dx.doi.org/10.1016/j.foodchem.2017.06.109

respond to appealing requirements, such as cost effectiveness (below 3 $ g^{-1} at the laboratory scale), environmental sustainability, and industrialization suitability. The SAMN@TA complex was tested on other species of foodborne bacteria prone to interact with tannic acid, leading to very promising results. At the same time, experiments are in progress to modify SAMNs with other polyphenols, showing bacteriostatic or bactericidal effects, and for testing the obtained nanoconjugates.

Concluding, the presented concept has an important validity and this paper represents the first example of this innovative approach.

Conflict of interest

All authors certify that there is no conflict of interests in this study.

Acknowledgments

Authors gratefully acknowledge CAPES (Brazil), process n. BEX 13160/13-3, University of Padua (Italy), Grant PRAT 2015 (progetti di Ateneo) n. CPDA159850, "Assegni di Ricerca Junior" 2014 n. CPDR148959 and CARIPARO Foundation for the support.

References

Baratella, D., Magro, M., Sinigaglia, G., Zboril, R., Salviulo, G., & Vianello, F. (2013). A glucose biosensor based on surface active maghemite nanoparticles. *Biosensors & Bioelectronics, 45*, 13–18.

Bettinsoli, L., Braga, L. M., Braga, R., Gatti, A., Magro, M., & Vianello, F. (2016). Apparatus and method for a separation through magnetic nanoparticles. Patent Application WO/2016/157027 A1.

Bohara, R. A., & Pawar, S. H. (2015). Innovative developments in bacterial detection with magnetic nanoparticles. *Applied Biochemistry Biotechnology, 176*, 1044–1058.

Bonaiuto, E., Magro, M., Baratella, D., Jakubec, P., Sconcerle, E., Terzo, M., et al. (2016). Ternary hybrid γ-Fe_2O_3/Cr^{VI}/amine oxidase nanostructure for electrochemical sensing: Application for polyamine detection in tumor tissue. *Chemistry – A European Journal, 22*, 1–8.

Buchanan, R. L., Gorris, L. G. M., Hayman, M. M., Jackson, T. C., & Whiting, R. C. (2016). A review of *Listeria monocytogenes*: An update on outbreaks, virulence, dose-response, ecology, and risk assessments. *Food Control, 75*, 1–13.

Cetin-Karaca, H. (2011). *Evaluation of natural antimicrobial phenolic compounds against foodborne pathogens* (Master's theses). University of Kentucky, paper 652.

Cetin-Karaca, H., & Newman, M. C. (2015). Antimicrobial efficacy of natural phenolic compounds against Gram positive foodborne pathogens. *Journal of Food Research, 4*, 14–27.

Cmiel, V., Skopalik, J., Polakova, K., Solar, J., Havrdova, M., Milde, D., et al. (2016). Rhodamine bound maghemite as a long-term dual imaging nanoprobe of adipose tissue-derived mesenchymal stromal cells. *European Biophysics Journal*. http://dx.doi.org/10.1007/s00249-016-1187-1.

Coppo, E., & Marchese, A. (2014). Antibacterial activity of polyphenols. *Current Pharmaceutical Biotechnology, 15*, 380–390.

Costadinnova, L., Hristova, M., Kolusheva, T., & Stoilova, N. (2012). Conductometric study of the acidity properties of tannic acid. *Journal of Chemical Technology and Metallurgy, 47*, 289–296.

David, J. R. D., Steenson, L. R., & Davidson, P. M. (2013). Expectations and applications of natural antimicrobials to foods. *Food Protection Trends, 33*, 241–250.

Fazary, A. E., Taha, M., & Ju, Y. H. (2009). Iron complexation studies of gallic acid. *Journal of Chemical & Engineering Data, 54*, 35–42.

Guivar, J. A. R., Martinez, A. I., Anaya, A. O., Valladares, L. D. L. S., Felix, L. L., & Dominguez, A. B. (2014). Structural and magnetic properties of monophasic Maghemite (γ-Fe_2O_3) nanocrystalline Powder. *Advances in Nanoparticles, 3*, 114–121.

Gyawali, R., & Ibrahim, S. A. (2014). Natural products as antimicrobial agents. *Food Control, 46*, 412–429.

Inbaraj, B. S., & Chen, B. H. (2015). Nanomaterial-based sensors for detection of foodborne bacterial pathogen and toxins as well as pork adulteration in meat products. *Journal of Food and Drug Analysis, 24*, 15–28.

Kim, S. Y., Kang, D. H., & Kim, J. K. (2011). Antimicrobial activity of plant extracts against *Salmonella Typhimurium*, *Escherichia coli* O157:H7, and *Listeria monocytogenes* on fresh lettuce. *Journal of Food Science, 76*, 41–46.

Kim, T. Y., Cha, S.-H., Cho, S., & Park, Y. (2016). Tannic acid-mediated green synthesis of antibacterial silver nanoparticles. *Archives Pharmacal Research, 39*, 465–473.

King, M., Lake, R., & Cressey, P. (2014). *Risk profile: Listeria monocytogenes in raw milk*. Christchurch, New Zealand: Institute of Environmental Science & Research.

Kiran-kumar, P. Badarinath, V., & Halami, P. (2008) Isolation of anti-listerial bacteriocin producing Lactococcus lactis CFR-B3 from Beans (Phaseolus vulgaris). The Internet Journal of Microbiology, 6.

Lagha, A. B., Dudonné, S., Desjardins, Y., & Grenier, D. (2015). Wild blueberry (*Vaccinium angustifoluim* Ait.) Polyphenols target *Fusobacterium nucleatum* and the host inflammatory response: Potential innovative molecules for treating periodontal diseases. *Journal of Agricultural and Food Chemistry, 63*, 6999–7008.

Li, G., Xu, Y., Wang, X., Zhang, B., Shi, C., Zhang, W., & Xia, X. (2014). Tannin-rich fraction from pomegranate rind damages membrane of *Listeria monoxytogenes*. *Foodborn Phathogenes Disease, 11*, 313–319.

Lim, C. K., Penesyan, A., Hassan, K. A., Loper, J. E., & Paulsen, T. (2013). Effect of tannic acid on the transcriptome of the soil bacterium *Pseudomonas protegens* Pf-5. *Applied Environmental Microbiology, 79*, 3141–3145.

Lomonaco, S., Nucera, D., & Filipello, V. (2015). The evolution and epidemiology of *Listeria monocytogenes* in Europe and the United States. *Infections, Genetics and Evolution, 35*, 172–183.

Magro, M., Sinigaglia, G., Nodari, L., Tucek, J., Polakova, K., Marusak, Z., et al. (2012a). Charge binding of rhodamine derivative to OH- stabilized nanomaghemite: universal nanocarrier for construction of magnetofluorescent biosensors. *Acta Biomaterialia, 8*, 2068–2076.

Magro, M., Faralli, A., Baratella, D., Bertipaglia, I., Giannetti, S., Salviulo, G., et al. (2012b). Avidin functionalized maghemite nanoparticles and their application for recombinant human biotinyl-SERCA purification. *Langmuir, 28*, 15392–15401.

Magro, M., Valle, G., Russo, U., Nodari, L., & F. Vianello. (2012c). Maghemite nanoparticles and method for preparing thereof. Patent Application WO/2012/010200.

Magro, M., Baratella, D., Pianca, N., Toninello, A., Grancara, S., Zboril, R., & Vianello, F. (2013). Electrochemical determination of hydrogen peroxide production by isolated mitochondria: A novel nanocomposite carbon-maghemite nanoparticle electrode. *Sensors and Actuators B: Chemical, 176*, 315–322.

Magro, M., Campos, R., Baratella, D., Lima, G. P. P., Hola, K., Divoky, C., et al. (2014a). A magnetically drivable nanovehicle for curcumin with antioxidant capacity and MRI relaxation properties. *Chemistry – A European Journal, 20*, 11913–11920.

Magro, M., Baratella, D., Salviulo, G., Polakova, K., Zoppellaro, G., Tucek, J., et al. (2014b). Core-shell hybrid nanomaterial based on prussian blue and surface active maghemite nanoparticles as stable electrocatalyst. *Biosensors & Bioelectronics, 52*, 159–165.

Magro, M., Baratella, D., Jakubec, P., Zoppellaro, G., Tucek, J., Aparicio, C., et al. (2015). Triggering mechanism for DNA electrical conductivity: Reversible electron transfer between DNA and iron oxide nanoparticles. *Advanced Functional Materials, 25*, 1822–1831.

Magro, M., Fasolato, L., Bonaiuto, E., Andreani, N. A., Baratella, D., Corraducci, V., et al. (2016a). Enlightening mineral iron sensing in *Pseudomonas fluorescens* by Surface Active Maghemite Nanoparticles: Involvement of the OprF porin. *Biochimica et Biophysica Acta – General Subjects, 1860*, 2202–2210.

Magro, M., Esteves, M. D., Bonaiuto, E., Baratella, D., Terzo, M., Jakubec, P., et al. (2016b). Citrinin mycotoxin recognition and removal by naked magnetic nanoparticles. *Food Chemistry, 203*, 505–512.

Magro, M., Bonaiuto, E., Baratella, D., de Almeida Roger, J., Jakubec, P., Corraducci, V., et al. (2016c). Electrocatalytic nanostructured ferric tannates: characterization and application of a polyphenol nanosensor. *ChemPhysChem, 17*, 3196–3203.

Magro, M., Domeneghetti, S., Baratella, D., Jakubec, P., Salviulo, G., Bonaiuto, E., ... Vianello, F. (2016d). Colloidal surface active maghemite nanoparticles for biologically safe Cr^{VI} remediation: From core-shell nanostructures to pilot plant development. *Chemistry – A European Journal, 22*, 14219–14226.

Mead, P. S., Slutsker, L., Dietz, V., McCraig, L. F., Bresee, S., Shapiro, C., et al. (1999). Food-related ilness and death in the United States. *Emerging Infectious Diseases, 5*, 607–625.

Miotto, G., Magro, M., Terzo, M., Zaccarin, M., Da Dalt, L., Bonaiuto, E., et al. (2016). Protein corona as a proteome fingerprint: the example of hidden biomarkers for cow mastitis. *Colloids and Surfaces B: Biointerfaces, 140*, 40–49.

Muñoz, P., Rojas, L., Bunsow, E., Sánchez-Cambronero, L., Alcalá, L., Rodríguez-Creixems, M., & Bouza, E. (2012). Listeriosis: An emerging public health problem especially among the elderly. *Journal of Infection, 64*, 19–33.

O'May, C., & Tufenkji, N. (2011). The swarming motility of *Pseudomonas aeruginosa* is blocked by cranberry proanthocyanidins and other tannin containing materials. *Applied Environmental Microbiology, 77*, 3061–3067.

Simões, M., Simões, L. C., & Vieira, M. J. (2010). A review of current and emergent biofilm control strategies. *LWT – Food Science and Technology, 43*, 573–583.

Sinigaglia, G., Magro, M., Miotto, G., Cardillo, S., Agostinelli, E., Zboril, R., et al. (2012). Catalytically active bovine serum amine oxidase bound to fluorescent and magnetically drivable nanoparticles. *International Journal of Nanomedicine, 7*, 2249–2259.

Skopalik, J., Polakova, K., Havrdova, M., Justan, I., Magro, M., Milde, D., et al. (2014). Mesenchymal stromal cell labeling by new uncoated superparamagnetic maghemite nanoparticles in comparison with commercial Resovist – An initial in vitro study. *International Journal of Nanomedicine, 9*, 5355–5372.

Tsai, T. H., Tsai, T. H., Chien, Y. C., Lee, C. W., & Tsai, P. J. (2008). In vitro antimicrobial activities against cariogenic streptococci and their antioxidante capacities: A comparative study of green tes versus different herbs. *Food Chemistry, 110*, 859–864.

Please cite this article in press as: de Almeida Roger, J., et al. Antimicrobial and magnetically removable tannic acid nanocarrier: A processing aid for *Listeria monocytogenes* treatment for food industry applications. *Food Chemistry* (2017), http://dx.doi.org/10.1016/j.foodchem.2017.06.109

Venerando, R., Miotto, G., Magro, M., Dallan, M., Baratella, D., Bonaiuto, E., et al. (2013). Magnetic nanoparticles with covalently bound self-assembled protein corona for advanced biomedical applications. *Journal of Physical Chemistry C, 117*, 20320–20331.

Waak, E., Tham, W., & Danielsson-Tham, M.-L. (2002). Prevalence and fingerprinting of *Listeria monocytogenes* strains isolated from raw whole milk in farm bulk tanks and in dairy plant receiving tanks. *Applied and Environmental Microbiology, 68*, 3366–3370.

Xiong, Q. R., Cui, X., Saini, J. K., Liu, D. F., Shan, S., & Jin, Y. (2014). Development of an immunomagnetic separation method for efficient enrichment of *Escherichia coli* O157:H7. *Food Control, 37*, 41–45.

Yu, W., & Xie, H. (2012). A review on nanofluids: preparation, stability mechanisms and applications. *Journal of Nanomaterials*. http://dx.doi.org/10.1155/2012/435873.

Please cite this article in press as: de Almeida Roger, J., et al. Antimicrobial and magnetically removable tannic acid nanocarrier: A processing aid for *Listeria monocytogenes* treatment for food industry applications. *Food Chemistry* (2017). http://dx.doi.org/10.1016/j.foodchem.2017.06.109

8-CONCLUSIONS

Nanotechnology have undoubtedly opened up enormous opportunities for innovative developments in the food industry, although challenges still persist. We demonstrated the selective purification of curcumin from a complex matrix (*C. longa* extract) by using uncoated magnetic nanoparticles, presenting a low cost platform for the efficient isolation of natural compounds. In this work we proposed a novel, nanoparticle based, high capacity purification system for polyphenols, characterized by short operating times and significant reduction of costs compared to traditional methods. Moreover, an industrial scale prototype for the magnetic purification of high value compounds from different raw materials is proposed. Furthermore, the possibility to apply SAMNs for the development of novel analytical devices, competitive to conventional detection systems, was assessed. The electrochemical properties of the SAMN@TA complex were used for the development of a novel nanosensor which was applied for the determination of polyphenols in real samples with high sensitivity and low detection limits. This results support future promising implementations of emerging technologies based on iron magnetic nanoparticles as viable platforms for improving food safety and quality. Finally, the antimicrobial properties of SAMN@TA were tested on *Listeria monocytog*enes in comparison with free TA. The similar bacteriostatic effects of both compounds demonstrated the preservation of the TA inhibitory activity when bound on nanoparticles toward *L. monocytogenes*, with the added value of magnetic driving ability of SAMN@TA, leaving no residues into the matrix. These features make this novel nanocarrier an innovative processing aid for surface treatments. Thus, SAMN@TA can be proposed as an effective, low-cost and environmentally friendly antimicrobial tool for food industry applications.

In conclusion, SAMNs can provide powerful instruments for magnetic separation, electrochemical sensors and antimicrobiological agents and can be applied in different biotechnological fields and in several production systems.

9-REFERENCES

Abouelmagd, S. A., Meng, F., Kim, B.-K., Hyun, H., & Yeo, Y. (2016). Tannic Acid-Mediated Surface Functionalization of Polymeric Nanoparticles. *ACS Biomaterials Science & Engineering*, *2*(12), 2294–2303. https://doi.org/10.1021/acsbiomaterials.6b00497

Ansari, F., Grigoriev, P., Libor, S., Tothill, I. E., & Ramsden, J. J. (2009). DBT Degradation Enhancement by Decorating Rhodococcus erythropolis IGST8 With Magnetic Fe3O4 Nanoparticles. *Biotechnology and Bioengineering*. https://doi.org/10.1002/bit.22161

Arakha, M., Pal, S., Samantarrai, D., Panigrahi, T. K., Mallick, B. C., Pramanik, K., … Jha, S. (2015). Antimicrobial activity of iron oxide nanoparticle upon modulation of nanoparticle-bacteria interface. *Scientific Reports*. https://doi.org/10.1038/srep14813

Azam, A., Ahmed, A. S., Oves, M., Khan, M. S., Habib, S. S., & Adnan, and M. (2012). Antimicrobial activity of metal oxide nanoparticles against Gram-positive and Gram-negative bacteria: a comparative study. *Int J Nanomedicine*, *7*, 6003–6009. https://doi.org/10.2147/IJN.S35347

Baratella, D., Magro, M., Jakubec, P., Bonaiuto, E., de Almeida Roger, J., Gerotto, E., … Korgel, B. (2017). Electrostatically stabilized hybrids of carbon and maghemite nanoparticles: electrochemical study and application. *Phys. Chem. Chem. Phys.*, *19*(18), 11668–11677. https://doi.org/10.1039/C7CP01486D

Baratella, D., Magro, M., Sinigaglia, G., Zboril, R., Salviulo, G., & Vianello, F. (2013). A glucose biosensor based on surface active maghemite nanoparticles. *Biosensors and Bioelectronics*, *45*(1), 13–18. https://doi.org/10.1016/j.bios.2013.01.043

Bhullar, K. S., & Rupasinghe, H. P. V. (2013). Polyphenols: Multipotent therapeutic agents in neurodegenerative diseases. *Oxidative Medicine and Cellular Longevity*. https://doi.org/10.1155/2013/891748

Bonaiuto, E., Magro, M., Baratella, D., Jakubec, P., Sconcerle, E., Terzo, M., … Vianello, F. (2016). Ternary Hybrid γ-Fe2O3/CrVI/Amine Oxidase Nanostructure for Electrochemical

Sensing: Application for Polyamine Detection in Tumor Tissue. *Chemistry - A European Journal*. https://doi.org/10.1002/chem.201600156

Bruce, P. G., Scrosati, B., Tarascon, J.-M., Chemie, A., & Bruce, P. G. (2008). Nanomaterials for Rechargeable Lithium Batteries**. *Angew. Chem. Int. Ed*, *47*, 2930–2946. https://doi.org/10.1002/anie.200702505

Buchanan, R. L., Gorris, L. G. M., Hayman, M. M., Jackson, T. C., & Whiting, R. C. (2017). A review of Listeria monocytogenes: An update on outbreaks, virulence, dose-response, ecology, and risk assessments. *Food Control*. https://doi.org/10.1016/j.foodcont.2016.12.016

Bülbül, G., Hayat, A., & Andreescu, S. (2015). Portable nanoparticle-based sensors for food safety assessment. *Sensors (Switzerland)*. https://doi.org/10.3390/s151229826

Burda, C., Chen, X., Narayanan, R., & El-Sayed, M. A. (2005). Chemistry and properties of nanocrystals of different shapes. *Chemical Reviews*. https://doi.org/10.1021/cr030063a

Chemello, G., Piccinetti, C., Randazzo, B., Carnevali, O., Maradonna, F., Magro, M., … Gigliotti, F. (2016). Oxytetracycline Delivery in Adult Female, *13*(6), 495–503. https://doi.org/10.1089/zeb.2016.1302

Chung, K.-T., Wong, T. Y., Wei, C.-I., Huang, Y.-W., & Lin, Y. (1998). Tannins and Human Health: A Review. *Critical Reviews in Food Science and Nutrition*, *38*(6), 421–464. https://doi.org/10.1080/10408699891274273

Etheridge, M. L., Campbell, S. A., Erdman, A. G., Haynes, C. L., Wolf, S. M., & McCullough, J. (2013). The big picture on nanomedicine: The state of investigational and approved nanomedicine products. *Nanomedicine: Nanotechnology, Biology, and Medicine*. https://doi.org/10.1016/j.nano.2012.05.013

Faraji, M. (2016). Recent analytical applications of magnetic nanoparticles. *Nanochem Res*, *1*(2), 264–290. https://doi.org/10.7508/ncr.2016.02.014

Gholami, A., Rasoul-Amini, S., Ebrahiminezhad, A., Abootalebi, N., Niroumand, U., Narges, E., & Younes, G. (2016). Magnetic properties and antimicrobial effect of amino and lipoamino acid

coated iron oxide nanoparticles. *MiNerVa BiotecNologica*, *28*(4), 177–186.

Ghosh, S., Banerjee, S., & Sil, P. C. (2015). The beneficial role of curcumin on inflammation, diabetes and neurodegenerative disease: A recent update. *Food and Chemical Toxicology*. https://doi.org/10.1016/j.fct.2015.05.022

Govan, J., & Gun 'ko, Y. K. (2014). Recent Advances in the Application of Magnetic Nanoparticles as a Support for Homogeneous Catalysts. *Nanomaterials*, *4*, 222–241. https://doi.org/10.3390/nano4020222

Green, C. E., Hibbert, S. L., Bailey-Shaw, Y. A., Williams, L. A. D., Mitchell, S., & Garraway, E. (2008). Extraction, processing, and storage effects on curcuminoids and oleoresin yields from Curcuma longa L. grown in Jamaica. *Journal of Agricultural and Food Chemistry*. https://doi.org/10.1021/jf073105v

Grumezescu, A., Mihaiescu, D., Chifiriuc, M., Lazar, V., Calugarescu, I., & Trainstary, V. (2010). In vitro assay of the antimicrobial activity of Fe3O4 and CoFe2O4 / oleic acid – core / shell on clinical isolates of bacterial and fungal strains. *Optoelectronics and Advance Materials - Rapid Communication*, *4*(11), 1798–1801.

Gupta, A. K., & Gupta, M. (2005). Synthesis and surface engineering of iron oxide nanoparticles for biomedical applications. *Biomaterials*. https://doi.org/10.1016/j.biomaterials.2004.10.012

Hola, K., Markova, Z., Zoppellaro, G., Tucek, J., & Zboril, R. (2015). Tailored functionalization of iron oxide nanoparticles for MRI, drug delivery, magnetic separation and immobilization of biosubstances. *Biotechnology Advances*. https://doi.org/10.1016/j.biotechadv.2015.02.003

Horák, D., Babič, M., Macková, H., & Beneš, M. J. (2007). Preparation and properties of magnetic nano- and microsized particles for biological and environmental separations. *Journal of Separation Science*. https://doi.org/10.1002/jssc.200700088

Hu, B., Liu, X., Zhang, C., & Zeng, X. (2017). Food macromolecule based nanodelivery systems for enhancing the bioavailability of polyphenols. *Journal of Food and Drug Analysis*. https://doi.org/10.1016/j.jfda.2016.11.004

Huang, Y. F., Wang, Y. F., & Yan, X. P. (2010). Amine-functionalized magnetic nanoparticles for rapid capture and removal of bacterial pathogens. *Environmental Science and Technology*. https://doi.org/10.1021/es102285n

Iqbal, A., Iqbal, K., Li, B., Gong, D., & Qin, W. (2017). Recent Advances in Iron Nanoparticles: Preparation, Properties, Biological and Environmental Application. *Journal of Nanoscience and Nanotechnology*, *17*(7), 4386–4409. https://doi.org/10.1166/jnn.2017.14196

Iranmanesh, M., & Hulliger, J. (2017). Magnetic separation: its application in mining, waste purification, medicine, biochemistry and chemistry. *Chem. Soc. Rev.* https://doi.org/10.1039/C7CS00230K

Ivanova, K., Fernandes, M. M., & Tzanov, T. (2013). Current advances on bacterial pathogenesis inhibition and treatment strategies. *Microbial Pathogens and Strategies for Combating Them: Science, Technology and Education*, (December), 322–36. https://doi.org/10.13140/RG.2.1.3988.7840

Jasieniak, J., Califano, M., & Watkins, S. E. (2011). Size-dependent valence and conduction band-edge energies of semiconductor nanocrystals. In *ACS Nano* (Vol. 5, pp. 5888–5902). https://doi.org/10.1021/nn201681s

Kafayati, M. E., Raheb, J., Angazi , Mahmoud Torabi Alizadeh, S., & Bardania, H. (2013). The effect of magnetic Fe3O4 nanoparticles on the growth of genetically manipulated bacterium, Pseudomonas aeruginosa (PTSOX4). *Iranian Journal of Biotechnology*, *11*(1), 41–46. https://doi.org/10.5812/ijb.9302

Kalkan, N. A., Aksoy, S., Aksoy, E. A., & Hasirci, N. (2012). Preparation of chitosan-coated magnetite nanoparticles and application for immobilization of laccase. *Journal of Applied Polymer Science*. https://doi.org/10.1002/app.34504

Kitts, D., & Weiler, K. (2003). Bioactive Proteins and Peptides from Food Sources. Applications of Bioprocesses used in Isolation and Recovery. *Current Pharmaceutical Design*, *9*(16), 1309–1323. https://doi.org/10.2174/1381612033454883

Knorr, D., Froehling, A., Jaeger, H., Reineke, K., Schlueter, O., & Schoessler, K. (2011). Emerging Technologies in Food Processing. *Annual Review of Food Science and Technology*, *2*(1), 203–235. https://doi.org/10.1146/annurev.food.102308.124129

Laurent, S., Forge, D., Port, M., Roch, a, Robic, C., Elst, L. V, & Muller, R. N. (2008). Magnetic Iron Oxide Nanoparticles: Synthesis, Stabilization, Vectorization, Physicochemical Characterizations, and Biological Applications (vol 108, pg 2064, 2008). *Chemical Reviews*, *108*(6), 2064–2110. https://doi.org/Doi 10.1021/Cr900197g

Livney, Y. D. (2015). Nanostructured delivery systems in food: Latest developments and potential future directions. *Current Opinion in Food Science*. https://doi.org/10.1016/j.cofs.2015.06.010

Lu, A. H., Salabas, E. L., & Schüth, F. (2007). Magnetic nanoparticles: Synthesis, protection, functionalization, and application. *Angewandte Chemie - International Edition*, *46*(8), 1222–1244. https://doi.org/10.1002/anie.200602866

Magro, M., Campos, R., Baratella, D., Lima, G., Hol??, K., Divoky, C., … Vianello, F. (2014). A magnetically drivable nanovehicle for curcumin with antioxidant capacity and MRI relaxation properties. *Chemistry - A European Journal*. https://doi.org/10.1002/chem.201402820

Magro, M., Faralli, A., Baratella, D., Bertipaglia, I., Giannetti, S., Salviulo, G., … Vianello, F. (2012). Avidin functionalized maghemite nanoparticles and their application for recombinant human biotinyl-SERCA purification. *Langmuir*. https://doi.org/10.1021/la303148u

Magro, M., Sinigaglia, G., Nodari, L., Tucek, J., Polakova, K., Marusak, Z., … Vianello, F. (2012). Charge binding of rhodamine derivative to OH - stabilized nanomaghemite: Universal nanocarrier for construction of magnetofluorescent biosensors. *Acta Biomaterialia*. https://doi.org/10.1016/j.actbio.2012.02.005

Magro, M., Valle, G., Russo, U., Nodari, L., & Vianello, F. (2012). Maghemite nanoparticles and method for preparing thereof, *2*(12). Retrieved from https://www.google.com/patents/US8980218

Mahmoudi, M., Sant, S., Wang, B., Laurent, S., & Sen, T. (2011). Superparamagnetic iron oxide

nanoparticles (SPIONs): Development, surface modification and applications in chemotherapy. *Advanced Drug Delivery Reviews*. https://doi.org/10.1016/j.addr.2010.05.006

Mai, T., & Hilt, J. Z. (2017). Magnetic nanoparticles: reactive oxygen species generation and potential therapeutic applications. *Journal of Nanoparticle Research*. https://doi.org/10.1007/s11051-017-3943-2

Martinez-Gutierrez, F., Olive, P. L., Banuelos, A., Orrantia, E., Nino, N., Sanchez, E. M., … Av-Gay, Y. (2010). Synthesis, characterization, and evaluation of antimicrobial and cytotoxic effect of silver and titanium nanoparticles. *Nanomedicine: Nanotechnology, Biology, and Medicine*, *6*(5), 681–688. https://doi.org/10.1016/j.nano.2010.02.001

Miklasińska, M., Kępa, M., Wojtyczka, R. D., Idzik, D., Dziedzic, A., & Wąsik, T. J. (2016). Catechin hydrate augments the antibacterial action of selected antibiotics against staphylococcus aureus clinical strains. *Molecules*. https://doi.org/10.3390/molecules21020244

Min, Walker, S., Tomita, G., & Anderson, R. C. (2008). Comparative antimicrobial activity of tannin extracts from perennial plants on mastitis pathogens. *Scientific Research and Essay*, *3*(2), 66–73. Retrieved from http://www.academicjournals.org/SRE

Miotto, G., Magro, M., Terzo, M., Zaccarin, M., Da Dalt, L., Bonaiuto, E., … Vianello, F. (2016). Protein corona as a proteome fingerprint: The example of hidden biomarkers for cow mastitis. *Colloids and Surfaces B: Biointerfaces*. https://doi.org/10.1016/j.colsurfb.2015.11.043

Molnár, Á., & Papp, A. (2017). Catalyst recycling—A survey of recent progress and current status. *Coordination Chemistry Reviews*, *349*, 1–65. https://doi.org/10.1016/j.ccr.2017.08.011

Musthaba, S. M., Baboota, S., Ahmed, S., Ahuja, A., & Ali, J. (2009). Status of novel drug delivery technology for phytotherapeutics. *Expert Opinion on Drug Delivery*, *6*(6), 625–637.

Pan, M.-H., & Ho, C.-T. (2008). Chemopreventive effects of natural dietary compounds on cancer development. *Chemical Society Reviews*. https://doi.org/10.1039/b801558a

Pankhurst, Q. A., Connolly, J., Jones, S. K., & Dobson, J. (2003). Applications of magnetic nanoparticles in biomedicine. *J. Phys. D: Appl. Phys*, *36*(3), 167–181.

Pathakoti, K., Manubolu, M., & Hwang, H.-M. (2017). Nanostructures: Current uses and future applications in food science. *Journal of Food and Drug Analysis*, *25*, 245–253. https://doi.org/10.1016/j.jfda.2017.02.004

Payne, D. E., Martin, N. R., Parzych, K. R., Rickard, A. H., Underwood, A., & Boles, B. R. (2013). Tannic acid inhibits staphylococcus aureus surface colonization in an isaA-dependent manner. *Infection and Immunity*. https://doi.org/10.1128/IAI.00877-12

Pérez-López, B., & Merkoçi, A. (2011). Nanomaterials based biosensors for food analysis applications. *Trends in Food Science and Technology*. https://doi.org/10.1016/j.tifs.2011.04.001

Raghupathi, K. R., Koodali, R. T., & Manna, A. C. (2011). Size-dependent bacterial growth inhibition and mechanism of antibacterial activity of zinc oxide nanoparticles. *Langmuir*. https://doi.org/10.1021/la104825u

Ramaswamy, V., Cresence, V. M., Rejitha, J. S., Lekshmi, M. U., Dharsana, K. S., Prasad, S. P., & Vijila, M. (2007). Listeria — review of epidemiology and pathogenesis. *J Microbiol Immunol Infect*, *40*, 4–13.

Roche, A., Ross, E., Walsh, N., O'Donnell, K., Williams, A., Klapp, M., … Edelstein, S. (2015). Representative literature on the phytonutrients category: Phenolic acids. *Critical Reviews in Food Science and Nutrition*, *57*(6), 1089–1096. https://doi.org/10.1080/10408398.2013.865589

Safarik, I., & Safarikova, M. (2004). Magnetic techniques for the isolation and purification of proteins and peptides. *Biomagnetic Research and Technology*, *2*(1), 7. https://doi.org/10.1186/1477-044X-2-7

Sinigaglia, G., Magro, M., Miotto, G., Cardillo, S., Agostinelli, E., Zboril, R., … Vianello, F. (2012). Catalytically active bovine serum amine oxidase bound to fluorescent and magnetically drivable nanoparticles. *International Journal of Nanomedicine*, *7*, 2249–2259. https://doi.org/10.2147/IJN.S28237

Skopalik, J., Polakova, K., Havrdova, M., Justan, I., Magro, M., Milde, D., … Zboril, R. (2014). Mesenchymal stromal cell labeling by new uncoated superparamagnetic maghemite nanoparticles in comparison with commercial Resovist--an initial in vitro study. *International Journal of Nanomedicine*. https://doi.org/10.2147/IJN.S66986

Taylor, E., & Webster, T. J. (2011). Reducing infections through nanotechnology and nanoparticles. *International Journal of Nanomedicine*. https://doi.org/10.2147/IJN.S22021

Tian, X., Zhang, L., Yang, M., Bai, L., Dai, Y., Yu, Z., & Pan, Y. (2017). Functional magnetic hybrid nanomaterials for biomedical diagnosis and treatment. *Wiley Interdisciplinary Reviews: Nanomedicine and Nanobiotechnology*. https://doi.org/10.1002/wnan.1476

Urbanova, V., Magro, M., Gedanken, A., Baratella, D., Vianello, F., & Zboril, R. (2014). Nanocrystalline iron oxides, composites, and related materials as a platform for electrochemical, magnetic, and chemical biosensors. *Chemistry of Materials*, *26*(23), 6653–6673. https://doi.org/10.1021/cm500364x

Valdés, M. G., González, A. C. V., Calzón, J. A. G., & Díaz-García, M. E. (2009). Analytical nanotechnology for food analysis. *Microchimica Acta*. https://doi.org/10.1007/s00604-009-0165-z

Varshney, M., Yang, L., Su, X.-L., & Li, A. Y. (2005). Magnetic Nanoparticle-Antibody Conjugates for the Separation of Escherichia coli O157:H7 in Ground Beef. *Journal of Food Protection*, *68*(9), 1804–1811.

Viswanathan, S., Radecka, H., & Radecki, J. (2009). Electrochemical biosensors for food analysis. *Monatshefte Fur Chemie*. https://doi.org/10.1007/s00706-009-0143-5

Wanninger, S., Lorenz, V., Subhan, A., & Edelmann, F. T. (2015). Metal complexes of curcumin – synthetic strategies, structures and medicinal applications. *Chem. Soc. Rev.* https://doi.org/10.1039/C5CS00088B

Whitesides, G. M. (2003). The “right” size in nanobiotechnology. *Focus on Nanobiotechnology*, *21*(10), 1161–1165.

Wu, L., Mendoza-Garcia, A., Li, Q., & Sun, S. (2016). Organic Phase Syntheses of Magnetic Nanoparticles and Their Applications. *Chemical Reviews*. https://doi.org/10.1021/acs.chemrev.5b00687

Xu, Y., Li, C., Zhu, X., Huang, W. E., & Zhang, D. (2014). APPLICATION OF MAGNETIC NANOPARTICLES IN DRINKING WATER PURIFICATION. *Environmental Engineering and Management Journal*, *13*(8), 2023–2029. Retrieved from http://omicron.ch.tuiasi.ro/EEMJ/

Yang, H., Qu, L., Wimbrow, A. N., Jiang, X., & Sun, Y. (2007). Rapid detection of Listeria monocytogenes by nanoparticle-based immunomagnetic separation and real-time PCR. *International Journal of Food Microbiology*. https://doi.org/10.1016/j.ijfoodmicro.2007.06.019